Università degli studi di Pisa
Facoltà di Ingegneria — Department of Engineering

Corso di Laurea Magistrale in — M.Sc. Course of

Ingegneria Meccanica — Mechanical Engineering

Design of High Field Solenoids made of High Temperature Superconductors

Thesis by

Antonio Bartalesi

Supervisors:

Prof. Ing. Marco Beghini

Dott. Ing. Emanuela Barzi

Degree year 2008-2009

To the memory of Francesco,
beloved cousin

LaTeX 2_ε

Abstract

This thesis starts from the analytical mechanical analysis of a superconducting solenoid, loaded by self-generated Lorentz forces. Also, a finite element model is proposed and verified with the analytical results. To study the anisotropic behavior of a coil made by layers of superconductor and insulation, a finite element meso-mechanic model is proposed and designed. The resulting material properties are then used in the main solenoid analysis.
In parallel, design work is performed as well: an existing Insert Test Facility (ITF) is adapted and structurally verified to support a coil made of $YBa_2Cu_3O_7$, a High Temperature Superconductor (HTS). Finally, a technological winding process was proposed and the required tooling is designed.

Acknowledgments

First of all I want to thank and express my gratitude to Emanuela Barzi, for believing in my skills and for granting me the possibility to do research on such an interesting and cutting edge subject such as high temperature superconductivity.
Her support has been sincere and continuous, making me always feel motivated, assisted, and at the same time free to follow my ideas, and focus on the aspects of the research I felt worth investigating.
I am really pleased to have been working together with Alexander Zlobin and the whole high-field magnet team at Fermilab: their world-class experience in the field of superconducting magnets fundamentally contributed to this thesis work, and to my personal professional growth.
A warm thank you goes also to the technicians of the Superconducting R&D laboratory: Marianne Bossert, Sean Johnson, Allen Rusy and Tom Van Raes. No experiment at all would have been possible without their precious skills and their experience.
A special acknowledgement goes to my professor Marco Beghini, in particular for teaching me the beautiful mechanical properties of anisotropic materials.
Thanks to my researcher colleagues Giuseppe Gallo, Andrea Latina, Vito Lombardo, Emanuele Terzini and Daniele Turrioni. Even if we have been working on different projects, they were always eager to discuss about our ideas and our results, helping me keep a broad view of the project and making our workplace a really enjoyable environment.
Thanks to Giuseppe for being the ideal housemate, thanks to Andrea for all the concerts, thanks Vito for being a reliable and trustworthy guide to the States, thanks Emanuele for being the best office mate I could ever have

asked.
Thanks to my family and to all my friends in the old world that kept in contact with me, despite of distance and time zones. Even if I was far apart I never felt separated from them.
Thank you all — grazie a tutti!

Chicago, IL
December the 16th, 2009

Antonio Bartalesi

Contents

List of Figures

Chapter 1

Introduction

1.1 High Temperature Superconductivity

Discovered in 1986 by Nobel Physic Prizes Karl Müller and Johannes Bednorz, High Temperature Superconductors [1] (abbreviated high-T_c or HTS) are materials that have a superconducting transition temperature (T_c) above 30 K, which was considered as the upper limit until the early eighties.
High Temperature has three common definitions in the context of superconductivity:

1. Above the temperature of 30 K that had historically been taken as the upper limit allowed by BCS theory [2]. This is also above the 1973 record of 23 K that had lasted until copper-oxide materials were discovered in 1986.

2. Having a transition temperature that is a larger fraction of the Fermi temperature [3] than for conventional superconductors such as elemental mercury or lead. This definition encompasses a wider variety of unconventional superconductors and is used in the context of theoretical models.

3. Greater than the boiling point of liquid nitrogen (77 K or −196 °C). This is significant for technological applications of superconductivity

because liquid nitrogen is a relatively inexpensive and easily handled coolant.

High temperature [3] superconductors (and other unconventional superconductors) differ in many important ways from conventional superconductors, such as elemental mercury or lead, which are adequately explained by the BCS theory.

Two decades of intense experimental and theoretical research, with over one hundred thousand published papers on the subject [4], has discovered many common features in the properties of HTS [5], but as of 2009 *there is no widely accepted theory to explain their properties.*

The question of how superconductivity arises in HTS is one of the major unsolved problems of theoretical condensed matter physics: the mechanism that causes the electrons in these crystals to form pairs is not known [5]. Despite intensive research and many promising leads, an explanation has so far eluded scientists. One reason for this is that the materials in question are generally very complex, multi-layered crystals, making theoretical modeling difficult.

However, not all the research done on HTS is theoretical: improving the quality and variety of samples also gives rise to considerable work, both with the aim of improving the characterization of the physical properties of existing compounds, as well as synthesizing new materials, often with the hope of increasing T_c.

Finally, technological research focuses on manufacturing HTS materials in sufficient quantities to make their use economically viable and optimizing their properties in relation to applications.

These materials in fact can be employed in many different projects, as all known high-T_c superconductors are Type-II superconductors [6]. In contrast to Type-I superconductors, which expel all magnetic fields due to the Meissner effect, Type-II superconductors allow magnetic fields to penetrate their interior in quantized units of flux; consequently, high-T_c superconductors can sustain much higher magnetic fields and therefore be suitable for the majority of practical applications.

Their main benefits are both the higher critical temperature being above the

boiling point of liquid nitrogen and also the higher critical magnetic field and critical current density at which superconductivity is destroyed. In magnet applications the high critical magnetic field is more valuable than the high-T_c itself.
However, HTS are brittle ceramics which are expensive to manufacture and not easily turned into wires or other useful shapes. Also, their layered chemical structure gives a directional dependence to the magnetic field response.

1.1.1 Cuprates superconductors

The term High Temperature Superconductor was used interchangeably with cuprate superconductor until iron based superconductors were discovered in 2006 [7]. The best known high-T_c superconductors are cuprates: yttrium barium copper oxide (YBCO, or $YBa_2Cu_3O_7$) and bismuth strontium calcium copper oxide (BSCCO, or $Bi_2Sr_2Ca_1Cu_2O_8$).
The cuprate superconductors adopt a perovskite structure, as shown in figure 1.1 and in figure 1.2. The copper-oxide planes are checkerboard lattices with squares of O^{2-} ions with a Cu^{2+} ion at the center of each square. The unit cell is rotated by 45° from these squares. Such materials are generally considered to be quasi two dimensional materials with their superconducting properties determined by electrons moving within the weakly coupled copper-oxide layers.
Neighboring layers containing ions such as La, Ba, Sr, or other atoms act to stabilize the structure and dope electrons or holes onto the copper oxide layers. Chemical formula of superconducting materials generally contain fractional numbers to describe the doping required for superconductivity. The undoped "parent" or "mother" compounds are Mott insulators with long-range antiferromagnetic order at low enough temperature. Single band models are generally considered to be sufficient to describe the electronic properties.
There are several families of cuprate superconductors and they can be named using the chemical symbol of the first element of the chemical formula followed by the numbers of all the elements of the formula, except oxygen. For

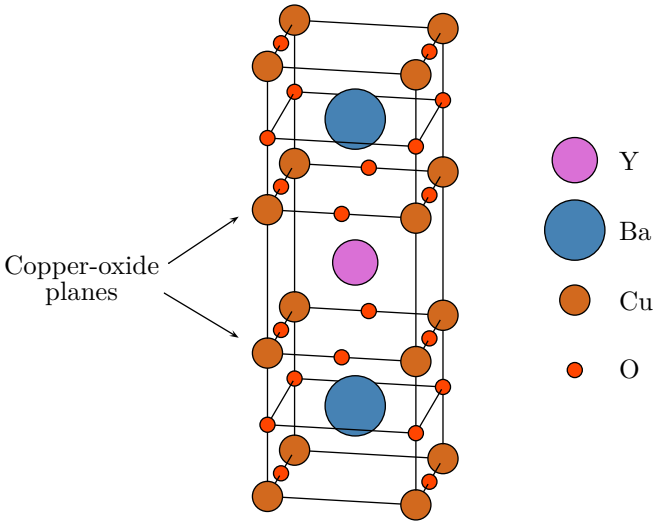

Figure 1.1: YBCO structure.

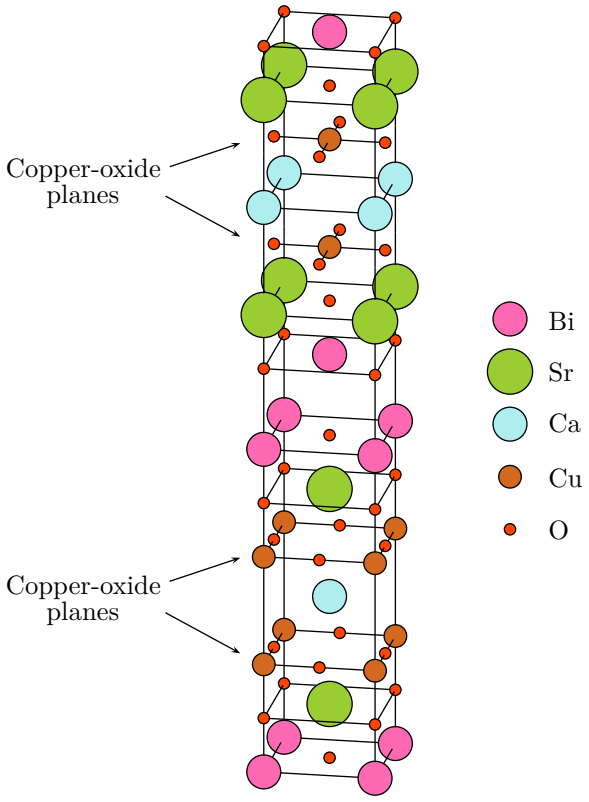

Figure 1.2: BSCCO Bi2212 structure.

example, YBCO ($YBa_2Cu_3O_7$) can alternatively be referred to as Y123 and BSCCO can be named Bi2201 or Bi2212 or Bi2223, depending on its chemical composition.

1.1.2 Iron-based superconductors

Iron-based superconductors (sometimes misleadingly called iron superconductors) are chemical compounds containing iron with superconducting properties. Interest in their superconducting properties began in 2006 with the discovery of superconductivity in LaFePO at 4 K [7] and gained much greater attention in 2008 after the analogous material LaFeAs(O,F) [8] was found to be superconductor at up to 43 K under pressure [9]. This is currently the family with the second highest critical temperature, behind the already mentioned cuprates.
Iron-based superconductors contain layers of iron and a "pnictogen" such as arsenic or phosphorus, or chalcogens. Figure 1.3 shows the structure of a proper iron-based HTS. In those materials, Fe-pnictide layers play a role analogous to the copper-oxygen planes in the HTS cuprates.
Since the original discoveries, several families of iron-based superconductors have emerged:

- LaFeAs(O,F) or $LaFeAsO_{1-x}$ with T_c up to 56 K, referred to as 1111 materials [10]. A fluoride variant of these materials was subsequently found with similar T_c values [11].

- (Ba,K)Fe_2As_2 and related materials with pairs of iron-arsenide layers, referred to as 122 compounds. T_c values range up to 38 K [12, 13]. These materials are also superconductors when iron is replaced with cobalt.

- LiFeAs and NaFeAs with T_c up to around 20 K. These materials are superconductors close to stoichiometric composition and are referred to as 111 compounds [14, 15, 16].

- FeSe with small off-stoichiometry or tellurium doping [17].

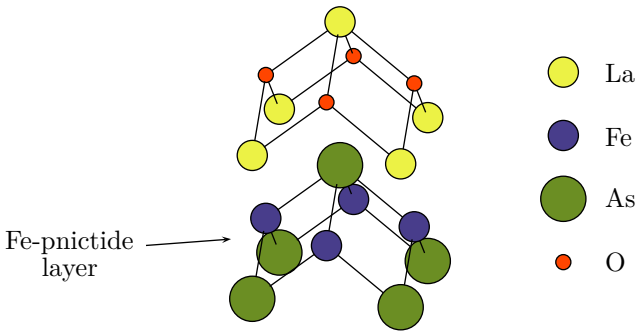

Figure 1.3: LaFeAsO structure.

Most undoped iron-based superconductors show a tetragonal-orthorhombic structural phase transition followed at lower temperature by magnetic ordering, similar to the cuprate superconductors [18]. However, they are poor metals rather than Mott insulators and have five bands at the Fermi surface rather than one. The phase diagram, emerging as the iron-arsenide layers are doped, is remarkably similar: the superconducting phase is close to, or overlaps, the magnetic phase. Strong evidence that the T_c value varies with the As-Fe-As bond angles has already emerged and shows that the optimal T_c value is obtained with undistorted $FeAs_4$ tetrahedra [19]. Much of the interest is because the new compounds are different in many aspects than the cuprates and may help lead to a theory of a non-BCS superconductivity.

1.1.3 Others High Temperature Superconductors

Magnesium diboride is occasionally referred to as a high-temperature superconductor because its T_c value of 39 K is above that historically expected for BCS superconductors. However, it is more generally regarded as the highest T_c conventional superconductor, the increased T_c resulting from two separate bands being present at the Fermi energy.

Fulleride superconductors [20] where alkali-metal atoms are intercalated into C_{60} molecules show superconductivity at temperatures of up to 38 K for Cs_3C_{60} [21].

Some organic superconductors and heavy fermion compounds are considered to be high-temperature superconductors because of their high T_c values rel-

ative to their Fermi energy, despite the T_c values being lower than for many conventional superconductors. This description may relate better to common aspects of the superconducting mechanism than the superconducting properties.
Theoretical work by Neil Ashcroft predicted that liquid metallic hydrogen at extremely high pressure should become superconducting at approximately room temperature because of its extremely high speed of sound and expected strong coupling between the conduction electrons and the lattice vibrations [22]. This prediction is yet to be experimentally verified.

1.1.4 Applications overview

The HTS technology is already being used with success in some relevant cases. Even if its application field is still object of investigation, here is a short list of the main usages as today:

Cellular communication

Superconducting filters in cellular base stations are the most advanced application of HTS films and various companies have placed commercial units on the market. Several thousand high frequency signal filters have been installed in the base-stations of cellular networks to improve their performance. Due to the low RF-resistance these filters offer the advantage of a lower noise level combined with sharp filter skirts which translates in higher selectivity and suppression of interference from other sources. The immediate benefits for network operators range from extended coverage to enhanced traffic and capacity per cell site. Consequently, the individual mobile phone user experiences better voice quality and fewer dropped calls. The extension of range can play an important role in rural areas or where GSM networks are upgraded to UMTS (3G filters) because these new networks usually require smaller cell size. The implementation of superconducting receiver front ends in mobile phone networks leads to a considerable reduction in the number of expensive base stations and consequent cost savings. As a matter of fact the installation of new antennas in urban areas is also getting increasingly

problematic because of inhabitants' resentments.

Satellite communication

Communication satellites are giant relay stations receiving weak signals from a station on earth and bouncing them back after amplification. The major part of the payload of such a satellite consists of RF-filters to select signals (calls, TV-programs) from a broadband transmission. After amplification signals are multiplexed and returned to a receiver on earth. Even considering cryogenics, superconducting filters offer the same performance as conventional filters at considerably smaller size and weight. This translates in cost saving rated at \$50 000/kg payload.

Fault current limiters (FCL)

Fault current limiters are protective units in the electric power grid. In case of short circuits, lightning strikes or whenever sudden excessive current bursts are threatening components of the grid, a fuse has to protect these components by switching off the network. Conventional circuit breakers are relatively slow and consequently the grid capacity has to be vastly oversized to withstand excess currents. Since conventional circuit breakers have to be serviced and reset manually, such faults result in long term blackouts. Superconducting fault current limiters are based on the principle that high temperature superconductors turn into a highly resistive state when a certain critical current is exceeded. This switching occurs within milliseconds and throttles down the excess current to the rated value. Hence, the grid is very effectively protected, existing capacities can be used better (smaller safety margins), and transformers can be saved when connecting grids. After the fault the FCL recovers within seconds and power outages can be avoided or are less severe.

Electric power cables

Transmission of electric power without losses is certainly the first idea when thinking about superconductivity. However, cables have to be flexible and

the use of high temperature superconductors which are ceramics is tricky. For some of the Bi-based HTS, a technology which produces HTS filaments embedded in a silver matrix is mature enough to produce kilometers of superconducting wire. It has been used to fabricate liquid nitrogen cooled cables which have been installed and successfully tested in many sites all over the world. The development of a new generation of so called 2G wire or coated conductors engaging YBCO is very much advanced and at the threshold of commercialization. YBCO offers better performance, reduced AC losses and the perspective of lower costs due to the lack of silver. However, the technical difficulties are immense since a high quality YBCO film on a metal tape requires more or less single crystalline (highly oriented) growth over hundreds of meters or even kilometers. A variety of manufacturing techniques has been developed, resulting in coatings on flexible metal tape with extremely high current carrying capability.

Magnetic resonance imaging (MRI)

Magnetic resonance imaging is a non-invasive medical diagnosis technique to detect for instance fractures of bones or sinews, or for cancer prevention. Unlike traditional radiography it does not expose the body to high energy radiation and reduces the risk of damages. It does not depend on the absorption of X-ray radiation, yields a completely different contrast and offers the advantage to investigate soft tissue structures as well. The quality of MRI images can be greatly enhanced by using superconducting RF-receiver coils. The receiving unit is realized in planar technology from thin films and can integrate coils and inter-digital capacitors to build an oscillating circuit tuned at the magnetic resonance frequency of the atomic nuclei which should contribute to the contrast of the image. Due to the compact geometry it is even possible to integrate several receiver units tuned to different frequencies to take images from various element distributions (H, Na, etc.) simultaneously.
The main advantage of the superconductor, however, lies in its low RF-losses (1000 times lower than copper). The high quality factor of the oscillator in-

creases the receiver sensitivity and results in an enhanced signal to noise ratio by at least one order of magnitude. As a consequence the sampling time to take a high resolution MRI image is greatly reduced. Superconducting receivers are essential for low field MRI, as they give the chance to build small and cheap open MRI systems, affordable not only for large clinics but also for single doctors (as orthopedists, vets, etc.) and in developing countries.

Squids

Superconducting quantum interference devices (SQuIDs) are extremely sensitive magnetic field sensors which have no parallel in conventional electronics and are based on the quantum effects which are responsible for superconductivity (Josephson effects). They are the most sensitive magnetic field sensors available to date.
Since every electrical current produces a magnetic field they can be used to monitor the tiniest current levels, generated for example in the human brain, or wherever nerves are transmitting signals through a body. Consequently, Squids can be used in medicine for remote recording of magneto cardiograms (MKG) or magneto encephalograms (MEG) with high spatial resolution. But also in other fields like material science and quality control; non-destructive evaluation (NDE) methods for metal pieces (as airplane components, tires, fuselage, etc.) to detect hidden flaws or fatigue cracks have been successfully demonstrated.

Nuclear magnetic resonance (NMR)

Nuclear magnetic resonance is an analytical tool which allows to determine the chemical composition and structure of complex chemical compounds like proteins. In order to get good resolution superconducting magnets are employed to produce the necessary high magnetic fields for the magnetic spitting of the RF signal. However, sensitivity and sampling time also depend on the noise of the RF receiver system. Superconducting antennas can considerably improve the signal to noise ratio by more than an order of magnitude. Consequently, the sampling time is greatly reduced and even very faint signals

can be detected.

Magnets

Superconductors are the only reasonable way to produce high magnetic fields necessary for research, in particle accelerators, and in medical and analytical tools like magnetic resonance imaging (MRI) and nuclear magnetic resonance (NMR) systems. Nowadays, such magnets employ conventional metallic superconductors like NbTi or Nb_3Sn operated at 4.2 K (liquid helium temperature) and at the limit of the material performance. HTS wires offer the chance to operate such magnets at higher temperatures and most importantly higher fields. YBCO coated conductors exhibit the best performances in terms of withstandable magnetic fields, and insert coils made of this material are periodically updating the world record of magnetic field intensity produced by steady state superconducting magnets.

1.1.5 Wire manufacturing

For the majority of possible superconductors' applications it is necessary to manufacture wires, tapes or cables. However, HTS have a brittle ceramic structure, which makes impossible any conventional drawing technique. The *powder in tube* process permitted to obtain the first HTS wires, using Bi2212. YBCO superconducting tapes were later obtained by deposition of a thin layer of YBCO onto an adequate substrate supported by a metal tape.

BSCCO wires and tapes

The powder in tube (PIT) process has been widely used to manufacture wire and tapes from brittle superconducting materials such as Nb_3Sn [23] or MgB_2 [24], and recently it is being adopted to produce both cuprate [25] and iron based [26] superconductors. Figure 1.4 shows a diagram of this process. In short, PIT consists in filling a metal tube with pulverized superconductor, then draw the tube into a wire, which can be used as is, or be additionally flattened into a tape.
In the case of BSCCO wires the initial metal tube is made of silver [27], and

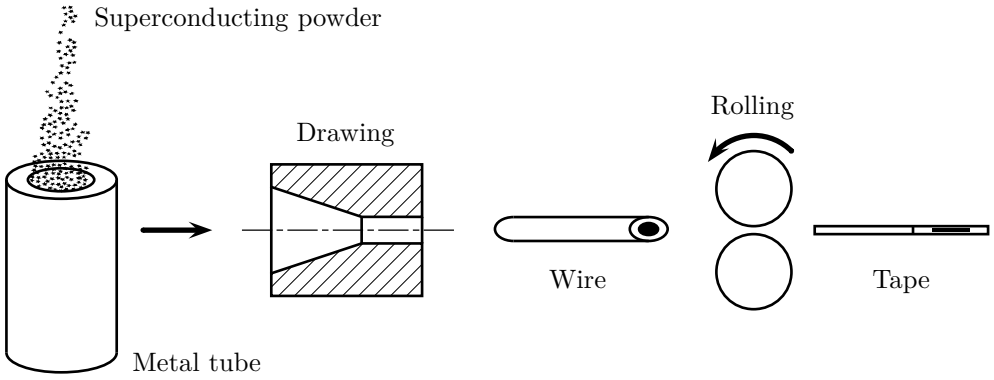

Figure 1.4: powder in tube process.

after the drawing phase a heat treatment in oxygen atmosphere is required, to react the powder and obtain the superconducting chemical structure [28]. Temperature in this phase reaches almost 890 °C [29], which results in an extremely oxidative atmosphere, limiting the material choice for the wires support.
Furthermore, the compound Bi2223 needs an additional deformation [30, 27], then after the drawing phase its wires are rolled into tapes.
Wires (or tapes) resulting from this process are not as flexible as conventional metal wire, especially after the heat treatment, which generates a rigid, brittle structure.
There are two ways of using such materials: they can be reacted and then carefully wound on relatively simple shapes or they can be wound in complex shapes and then reacted [31]. The second option gives better results at a higher cost, because only a few materials are able to support BSCCO during the oxygen heat treatment, and they are expensive and hard to machine.

YBCO tapes

PIT is not a reliable process to obtain YBCO wires [32], however, it is possible to obtain superconducting tapes by thin-film deposition of superconductor onto an adequate substrate supported by a metal tape. To achieve this, two industrial processes are currently adopted: Rolling-Assisted Biaxially-Textured Substrates (RABiTS) [33] and Ion Beam Assisted Deposition (IBAD) [34].

Two companies are currently producing and selling useful amounts of YBCO tapes: American Superconductor Corp. and Superpower Inc., both based in the USA.
American Superconductor tapes are made with the RABiTS process [35], and are sold in three different finishings: copper stabilized (type 344C), stainless steel stabilized (type 344S) and brass stabilized (type 344B). For every kind of tape, the width is 4.41 ± 0.14 mm, while the average thickness is 0.2 mm for the 344C type, 0.3 mm for the 344S type and 0.4 mm for the 344B type. Maximum current is in the order of 100 A, in every case.
Superpower tapes, made with the IBAD process, show substantially better properties [36] and a wider range of dimensions. As figure 1.5 shows, those tapes have a hastelloy C-276 core, which strongly improves the overall mechanical resistance of the tape itself, pushing the ultimate tensile stress above 700 MPa at 4.2 K. This core is covered with several substrate layers, which allow the growth of a thin layer (1 µm thick) of YBCO oriented crystals. Finally, a last layer of silver and the optional Surround Copper Stabilization, or SCS, are applied to completely encase the tape. Thickness varies from 0.055 mm to 0.1 mm, depending on the presence of SCS. An optional 0.105 mm thick, non-stabilized tape is also available: this configuration is obtained by using a 100 µm thick hastelloy tape, instead of the usual 50 µm thick tape. Nominal widths for those tapes are 3, 4, 6 and 12 mm. Minimum critical current in 4 mm wide tapes ranges from 80 to 110 A at 77 K. This value substantially increases at 4.2 K, reaching 1200 A for short-length sample of tapes [37].

1.2 The next generation accelerators

With the recent restart of the Large Hadron Collider at CERN occurred in November 2009, the short attention span of the world has already turned to the next "big thing".
One of the major proposals as a successor to the Large Hadron Collider is the *Muon Collider* [38, 39, 40] being proposed by Fermilab [41]. The collider would accelerate muon particles, which are about 200 times heavier than

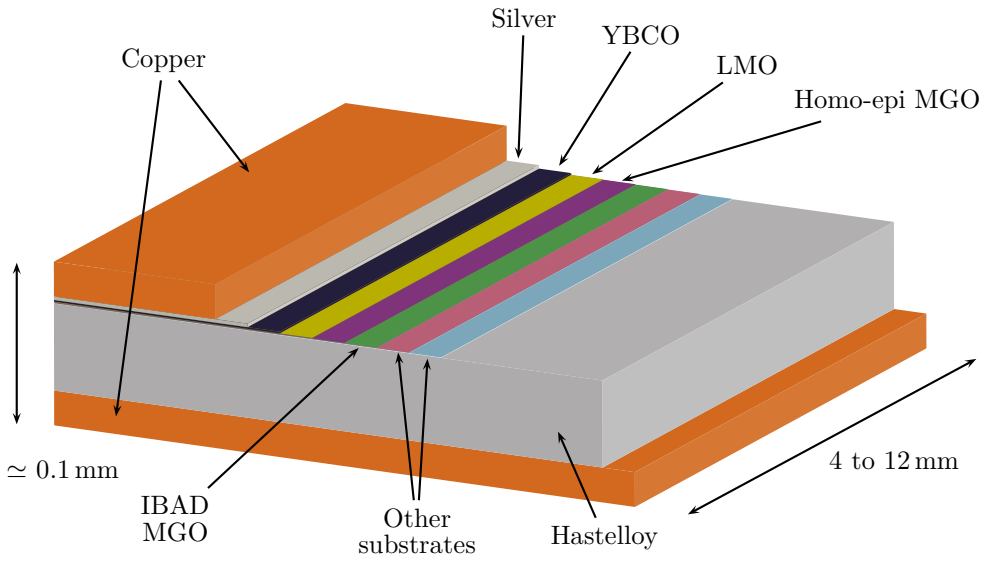

Figure 1.5: YBCO tape obtained with the IBAD process.

electrons, into beams that would collide with each other, creating interactions more energetic than electron collisions. A benefit of muons over electrons is that, since they are heavier, they will not emit as much electromagnetic radiation (and lose as much energy) when going around a circular accelerator ring. Such an accelerator could be built in the existing Fermilab facility.
A most recent idea, the *Neutrino Factory* [42, 43, 44, 45, 46, 47, 48] has also been proposed. Such an accelerator has been shown to deliver unparalleled performance in studying neutrino mixing and has tremendous sensitivity to new physics in the neutrino sector [49, 50]. Muons decaying in a storage ring constitute in fact a unique source of well-characterized electron and muon neutrinos and antineutrinos.
In conclusion, Muon Collider (MC) and Neutrino Factory (NF) are attractive options for future facilities aimed at achieving the highest lepton-antilepton collision energies and precision measurements of parameters of the neutrino mixing matrix. Mc and NF accelerators complexes are shown schematically in figure 1.6 and 1.7, respectively.
At the front-end both NF and MC require similar, perhaps identical, intense muon sources, and hence there is significant overlap in NF and MC R&D. The muon source is designed to deliver about 10^{21} low energy muons per year

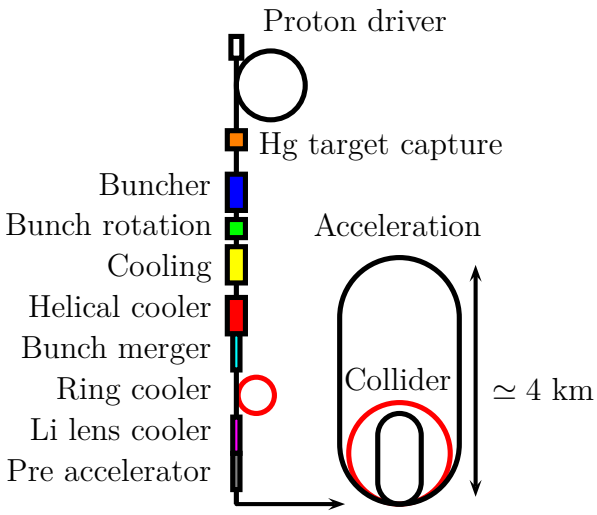

Figure 1.6: schematic of 1.5 TeV Muon Collider.

within the acceptance of an accelerator, and consists of:

1. A multi-MW proton source delivering a multi-GeV proton beam onto a pion production target.

2. A high-field target solenoid that radially confines the secondary charged pions.

3. A long solenoidal channel in which the pions decay to produce positive and negative muons.

4. A system of RF cavities that capture the muons in bunches and reduce their energy spread (phase rotation).

5. A muon ionization cooling channel that reduces the transverse phase space occupied by the beam by a factor of a few in each transverse direction.

At this point the beam will fit within the acceptance of an accelerator for a NF. However, to obtain sufficient luminosity, a MC requires further muon cooling. In particular, the 6D phase-space must be reduced by a factor 10^6, which requires a longer and more ambitious cooling channel. Finally, in both NF and MC schemes, after the cooling channel the muons are accelerated

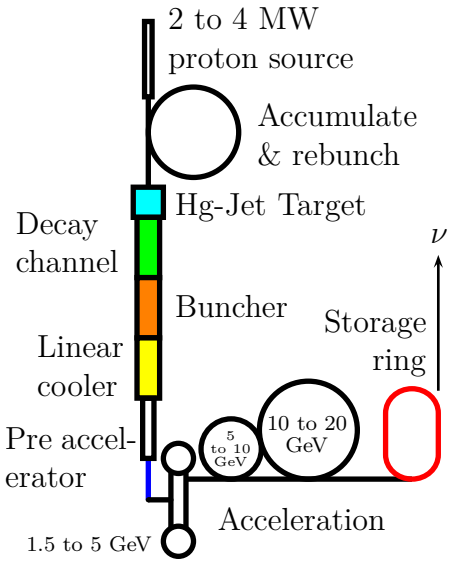

Figure 1.7: schematic of 20 GeV Neutrino Factory.

to the desired energy and injected into a storage ring. In a NF the ring has long straight sections in which the neutrino beam is formed by the decaying muons. In a MC, positive and negative muons are injected in opposite directions and collide for about 1000 turns before the muons decay.

1.2.1 Current status

The first detailed Muon Collider study [39] has been conducted in 1995. This study assesses the physics program, specifies the required collider parameters, and assesses the feasibility of achieving these parameters. The study concludes that:

1. For a Muon Collider with $\sqrt{s} = 1\,\text{TeV}$ to a few TeV, the required luminosity is 10^{34} to $10^{35}\,\text{cm}^{-2}\,\text{s}^{-1}$.

2. Muon Colliders providing this luminosity seem plausible, but require an aggressive R&D program.

In 1997, the Neutrino Factory and Muon Collider Collaboration (NFMCC) has been formed and has begun to receive support to pursue the required

R&D program. Further studies by the NFMCC have identified, as the most challenging of the things needed before Muon Colliders can be considered viable, the design of a muon cooling channel to cool the initial muon beam in 6D phase space by about a factor of 10^6. Other challenges include the design of a suitable proton driver, the development of the required target technology, the design of cost-effective bunching, phase rotation, and acceleration systems, and the design of the collider ring. In recent years there has been significant progress. In particular:

1. Suitable multi-MW proton sources have been studied in the context of the future U.S., European, and Japanese particle physics programs (e.g. an 8 GeV superconducting H^- linear accelerator providing a 2 MW beam at Fermilab).

2. A liquid Hg-jet target concept has been developed and the proof-of-principle was demonstrated by the experiment MERIT in 2008.

3. Cost-effective bunching and phase rotation channels have been successfully designed for Neutrino Factories. These designs are believed to also be suitable for Muon Colliders.

4. Muon cooling R&D for the initial stages of a Muon Collider cooling channel has advanced, and a cooling channel demonstration experiment (MICE) is in preparation.

5. The NFMCC and Muons Inc. have made a conceptual breakthrough in design concepts for a complete Muon Collider cooling channel. In the last four years the first complete self-consistent design for the required channel has emerged.

Muon Collider R&D activities are pursued by the NFMCC and by Muons Inc. The main focus of the NFMCC is to meet its commitments to MERIT and MICE, two crucial experiments for the R&D program. The NFMCC also provides people for design and concept development. Muons Inc. complements the NFMCC effort, focusing mainly on design and concept development. Given the recent progress by Muons Inc. and NFMCC, two new activities, requiring additional resources, are focusing on:

- Take a fresh look at the overall Muon Collider design, identify the outstanding R&D issues not being addressed by the ongoing R&D program and formulate a longer term R&D plan to address these issues.
- Develop and test the critical components needed to implement a complete Muon Collider cooling channel.

A proposal [51] is to conduct this R&D in close collaboration with the NFMCC and Muons Inc. Their design studies will focus on a $\sqrt{s} = 1.5\,\text{TeV}$ Muon Collider, and will build on and complement earlier NFMCC studies for 100 GeV and 3 to 4 TeV colliders [40].

Breakthrough in cooling channel ideas

To maximize the Muon Collider luminosity it is desirable that, in each cycle, all of the muons of a given sign are captured within a single bunch. Therefore, in the initial Muon Collider cooling channel designs, all of the muons were captured into one, or at most two, bunches, and then cooled and accelerated. However, detailed simulations have shown that a cooling channel based on this concept is difficult to implement using realistic hardware. Despite several years of work, a complete Muon Collider cooling scheme for muons captured within one or two bunches has not emerged. On the other hand, cooling channel designs for a Neutrino Factory, in which the muons are captured within a long bunch train, have been successful. Note that, in contrast to the initial Muon Collider designs, in a Neutrino Factory the initial muon population is captured into many bunches, and hence each bunch within the train occupies a smaller longitudinal phase-space (energy spread and bunch length). This facilitates the use of higher frequency RF in the cooling channel, and hence higher accelerating gradients and smaller RF cavities. In 2006 a new Muon Collider cooling channel concept has been explored. In the new design the early part of the muon cooling channel resembles (and at present is identical to) a Neutrino Factory cooling channel. The muons passing through this channel are captured within a bunch train, enabling the use of "high frequency" (805 MHz) RF. Only after a large amount of longitudinal cooling are the muons captured into a single bunch. Cooling

is then continued to achieve the desired final emittance. In this way, high frequency RF can be used throughout the cooling channel. The new concept has resulted in the first Muon Collider cooling scheme that uses plausible hardware and takes the muons from their initial emittance to the desired final emittance. In addition to this conceptual breakthrough, in the last two years new cooling channel component concepts have emerged. The more promising of the new ideas include using:

1. RF cavities filled with high pressure gas.
2. Very high field solenoids based on the developing HTS conductor technology.
3. More complex magnetic channels that provide helical motion of the bunches as they propagate down the channel.

1.2.2 High Field Magnets project at Fermilab

The ability of High Temperature Superconductors to carry high currents in presence of strong magnetic fields makes those materials the best candidates to build the high field magnets that will be required by the next generation accelerators.
However, in most cases it is not convenient to build entire magnets with HTS, because of the higher cost and the technical disadvantages of this material: HTS usage can be limited to the regions of the magnet exposed to magnetic fields that are beyond the limits of traditional superconductors. For this reason the most common solutions are multi-material hybrid magnets, which in case of solenoids means HTS insert magnets.
One of the goals of the High Field Magnets project at Fermilab (HFM) is to build a HTS insert solenoid and test it in high values of self-field and background field, to demonstrate the feasibility of such magnets.
Part of the HFM project, the Superconducting R&D Group of the Fermilab Technical Division is currently studying, characterizing and building HTS made wires, cables and a prototypical insert solenoid. One of its goals is to

provide HTS knowledge, in terms of physical properties and technological know-how, to the HFM project.

1.3 Definition of the thesis work

Among many other activities, the Superconducting R&D group at Fermilab is building an insert coil made of HTS YBCO tape, as well as a probe to support, energize and monitor the solenoid itself.
This activity is referred to as the Insert Test Facility (ITF) project, and purpose of this thesis work is to advance toward the manufacturing of HTS solenoids, by verifying and putting in commission the ITF, and also designing the tooling necessary to wind HTS solenoids.

1.3.1 Previous situation

At the time this thesis work started, the ITF project has already been going on for about a year, and much of the design parameters were already frozen. Several important decisions regarding the dimensions and the layout of the insert and its probe were already taken, nevertheless an additional effort was required to put the ITF in commissioning, as the winding process, the soldering method, the mechanical stresses handling and the probe layout still presented some issues.

The outer magnet

The magnet dedicated to provide the background field for this project is a 14 T Nb_3Sn-NbTi hybrid superconducting magnet system made by Oxford Instruments®: the Teslatron® II. Such system has a cold bore of 77 mm and a maximum useful height of about 170 mm, which correspond to the height of the shortest coil of the magnet system itself.

Insert coil design

The superconducting tape to be used for the manufacture of the insert coil and the dimensions of the coil itself have already been defined by the previous analyses, taking into account the magnetic and electrical limits of the superconductor:

- Superpower Inc. SCS4050 YBCO tape (section of 4 mm × 0.1 mm).
- Kapton® insulation (section of 4.5 mm × 25.4 µm).
- Operating current 294 A.
- Coil inner radius 9.5 mm.
- Coil outer radius 31 mm.
- Coil height 126 mm.

It has been proposed to obtain the whole insert coil by assembling a series of 14 double pancake units (see figure 1.8).
Such units are composed by two spirals of superconductor, positioned one on top on the other and sharing the same axis. One spiral is clockwise, while the other is counter-clockwise, and they are connected at their inner radius. The pancake design is chosen because it is considered the best way to obtain a solenoid using a tape shaped conductor, while the *double* pancake design allows to obtain units made of a single piece of tape, which can be piled and joined together by splicing the superconductor tape only at their outer radius: there are no joints to be made at the inner radius of the coil. For obvious reasons, it would have been extremely difficult to solder together two pieces of tape laying at the inner radius of a wound coil, having an inner radius as small as 9.5 mm, therefore the convenience of the double pancake units solution.
With those design options, a structural analysis has already been performed, however the assumptions that were made at the beginning of that analysis need to be revised. In particular one hypothesis does not seem correct: the non-detachment of the coil from its winding kernel despite of a centrifugal-like loading due to Lorentz forces.

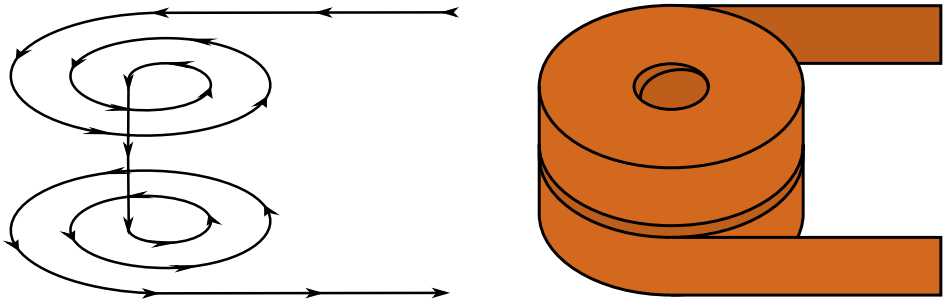

(a) schematic of a double pancake coil. (b) aspect of a double pancake coil.

Figure 1.8: the double pancake unit.

The ITF probe

The prototype of a testing probe, designed to hold the insert coil in place inside the Teslatron II, has been manufactured, but it was not completed at the beginning of this work, as it needs further modifications in order to be put in commissioning.

Winding tooling

Finally, when this thesis started, there was no way to manufacture any double pancake unit, except from the hand-crafting of very thin coils (two or three turns of superconducting tape per spiral); while it is obvious that a machine assisted winding is indispensable to obtain double pancake units of the previously defined dimensions.

1.3.2 Objectives

In conclusion, in order to proceed with the manufacturing and testing of the first YBCO insert coil of such dimensions by the Fermilab superconducting R&D group, the following objectives are assigned to this thesis work:

1. The design of a structure to constrain the solenoid expansion and keep its mechanical stresses below an acceptable level.

2. A more accurate mechanical analysis, to investigate further into the

complex mechanical behavior of a coil made of several different materials wound together.

3. The verification of the ITF probe, and its eventual modification in order to be put in commissioning.

4. The design of the tooling necessary to wind a double pancake unit of the required dimensions.

Each chapter of this thesis describes in detail how each of the above objectives has been pursued.

Chapter 2

The insert solenoid support

The very first task of this thesis work consists in finding an adequate solution to constrain the solenoid against its expansion due to Lorentz forces, requiring a first estimate of the resulting stresses.
Considering all the limitations in space and in materials, a *stainless steel wrap* on the outer surface of the coil is being proposed for the coil support, as it is thought to be the most convenient solution: such constrain is easy to manufacture, relatively inexpensive, compact, and it is also possible to optimize the amount of stainless steel wire to wind around the solenoid as well as its tension during the winding (to obtain a *pre-stress* compression state in the coil).
The easiest and more reliable way to obtain a first estimate of the mechanical loads occurring inside the superconducting coil and its outer wrapping is an analytical model. Such analysis occurs in three steps:

1. Calculation of the magnetic field generated by the insert coil and outer magnet.

2. Computation of Lorentz forces.

3. Structural analysis and stress evaluation.

2.1 Magnetic field of a solenoid

The first step is the definition of an analytical model to represent the magnetic field generated by a cylindrical solenoid. The coil can be approximated to a hollow cylindrical solid, having inner radius a, outer radius b and height $2l$, as shown in figure 2.1. The solenoid has an average current density J:

$$J = \frac{iN}{2l\,(b-a)} \tag{2.1}$$

in which i is the current flowing through a wire and N is the number of turns. The current density J is also obtained by:

$$J = \frac{i}{A} \tag{2.2}$$

where A is the overall area of the tape cross section, with insulation.
Considering the Biot-Savart law for the magnetic field generated by an electric current flowing into a wire, and integrating for a finite length cylindrical solid [52], the magnitude of the magnetic field B_0 at the center of the solenoid is obtained by the following:

$$B_0 = JaF\,(\alpha, \beta) \tag{2.3}$$

Where $\alpha = b/a$, $\beta = l/a$ and

$$F\,(\alpha, \beta) = \mu_0 \beta \ln \left[\frac{\alpha + (\alpha^2 + \beta^2)^{\frac{1}{2}}}{1 + (1 + \beta^2)^{\frac{1}{2}}} \right] \tag{2.4}$$

For the first magneto-mechanical analysis, equation 2.3 offers a valid estimate of the magnetic field that occurs at the center of the solenoid. The insert coil however is a three-dimensional object, so the generated field should be expressed by function of z, r and θ. Luckily two dimensions can be simplified for the whole analytical analysis:

1. The whole model is axial-symmetric, so there are no dependencies with respect to the angular variable θ.

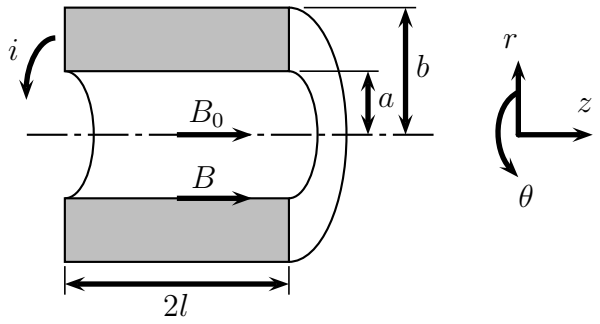

Figure 2.1: schematic of the solenoid.

2. Hypothesizing a "long" solenoid the effect of z is negligible: the section that lies at the middle of the coil can be studied, with the assumption that the solenoid behaves in the same way along its whole length[1].

Additionally, the field of the insert solenoid is assumed to be always parallel to the coil axis z, so its direction is fixed, and only one equation is needed to fully characterize it: a scalar function of the radius: $B_s(r)$.
As further approximation, it is imposed that the value of the magnetic field at the center of the solenoid B_0 and the value of field at the inner radius are the same:

$$B_0 = B_s(a) \tag{2.5}$$

Also, the field decreases linearly with the growth of the radius, reaching the value of zero at the outer radius of the solenoid, and remaining zero beyond it. In synthesis:

$$B_s(r) = \begin{cases} B_0 & \text{for } |r| \leq a \\ \frac{B_0 b}{b-a} - \frac{B_0}{b-a} r & \text{for } a < |r| < b \\ 0 & \text{for } |r| \geq b \end{cases} \tag{2.6}$$

Since there are no ferromagnetic parts, the magnetic field of the insert solenoid can be simply added to the one of its surrounding magnet system, to

[1]This assumption is confirmed to be correct by the finite element model, which takes into account the z dimension, as described in Chapter 3. The points $z = 0$, $r = a$ are in fact exposed to the highest value of magnetic field that occurs in the whole coil.

obtain:

$$B(r) = B_s(r) + B_e \tag{2.7}$$

In this equation B_e is the magnetic field magnitude generated by the external magnets, and can be considered as a *background field* which is constant in every point of the test coil, and always directed like the *self-field* generated by the insert.
As last assumption, in fact, the self-field and the background field always have the same sense (as they are powered with the same polarity) and direction.
Since the dimensions of the insert solenoid are known, as well as its operating current and the value of background field, the required value of the shape factor $F(\alpha, \beta)$ and the current density J can be easily determined, so that the equation 2.7 is fully defined.

2.2 Mechanical model of the solenoid

For the very first mechanical analysis the hypotheses are the following:

1. Homogeneous material.
2. Linear material.
3. Elastic material.
4. Isotropic material.

These may appear unrealistic, as the solenoid and its outer wrapping are made by wound tape and wire, which are not solid continuous materials. However, the fact that the coil is proposed to be impregnated with epoxy resin, cured, and tightened with its outer steel wrap, encourages the continuous hypothesis. Results still need to be checked, and in particular it is necessary to consider that without adhesives, a coil is not able to be in tension in the radial direction, as this would cause the detachment of adjacent wound layers. This is only possible because these layers are joined with resin, and in case the epoxy would not be strong enough, this load condition should be avoided by tightening the stainless steel wrapping.

Following the standard techniques [53] for axial-symmetric disc axial-symmetrically loaded, and referring to notation represented in figure 2.2, the Lamé equation is obtained:

$$\frac{\mathrm{d}}{\mathrm{d}r}\left\{\frac{1}{r}\left[\frac{\mathrm{d}}{\mathrm{d}r}(ur)\right]\right\} = -\frac{1-\nu^2}{E}JB(r) \tag{2.8}$$

Where u is the local displacement in the radial direction, ν is the Poisson's ratio and E is the Young's modulus. The term $JB(r)$ represents the Lorentz force acting on the infinitesimal part of the disc. Being the magnetic field and the current directed respectively along the z axis and the θ direction, the only resulting components from their vector product is radial, and its intensity is equal to $JB(r)$.
After solving 2.8 in the u variable, the circumferential or hoop stress $\sigma_{\theta\theta}$ and the radial stress σ_{rr} are obtained by the following:

$$\varepsilon_{\theta\theta}(r) = \frac{u}{r}$$

$$\varepsilon_{rr}(r) = \frac{\mathrm{d}u}{\mathrm{d}r}$$

$$\sigma_{\theta\theta}(r) = \frac{E}{1-\nu^2}\left[\varepsilon_{\theta\theta}(r) + \nu\varepsilon_{rr}(r)\right] \tag{2.9}$$

$$\sigma_{rr}(r) = \frac{E}{1-\nu^2}\left[\varepsilon_{rr}(r) + \nu\varepsilon_{\theta\theta}(r)\right] \tag{2.10}$$

Finally, the axial stress σ_{zz} is evaluated according to the generalized plain strain theory, which is thought to be the most representative, considering that the solenoid behaves as a "long" solid (as already assumed in the magnetic model):

$$\overline{\sigma}_{zz} = \frac{2\int_a^b \nu\left[\sigma_{\theta\theta}(r) + \sigma_{rr}(r)\right] r\,\mathrm{d}r}{b^2 - a^2} \tag{2.11}$$

and:

$$\sigma_{zz}(r) = \nu\left[\sigma_{\theta\theta}(r) + \sigma_{rr}(r)\right] - \overline{\sigma}_{zz}$$

In the above $\overline{\sigma}_{zz}$ is the average axial stress while $\sigma_{zz}(r)$ expresses the axial stress in function of the radius.

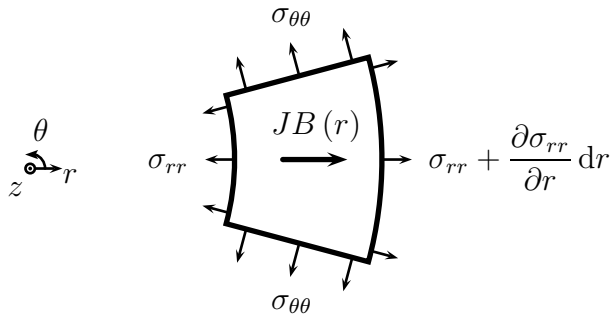

Figure 2.2: infinitesimal element.

However, regarding σ_{zz}, it is worth to point out that there is a small component in the Lorentz forces that compresses the solenoid along its axis. This compression is caused by a small radial component of the magnetic field seen at the upper and lower extremities of the coil, and therefore it does not appear in this simplified model. Its effect is negligible at this stage of the analysis, but it will be noticeable when comparing the values of σ_{zz} obtained with the analytical and finite element models. By a physical point of view, those forces now neglected are the ones that are responsible of the north-south attraction between energized coil ends, and their resultant can be strongly seen if the solenoid in not perfectly centered at the center of the outer magnet, as in that case the two coils would try to re-align themselves.

2.2.1 Mechanical constraints

As expected for a solenoid, its most important constraint is on the outer cylindrical surface. The filamentous nature of the coil itself and the loading caused by Lorentz forces, which tend to radially expand the solenoid, make almost impossible to constrain it in a different way than keeping it together by its external radial surface. For this reason the only constraint considered in this analysis is on the outer radius of the coil. Figure 2.3 shows the solenoid, its loading and its radial support (called *skin* from now on).
The skin can be modeled either as perfectly rigid or elastic: the first case represents the best possible constrain, and it is considered as the ideal case (besides pre-stress); the second represents better the behavior of a stainless

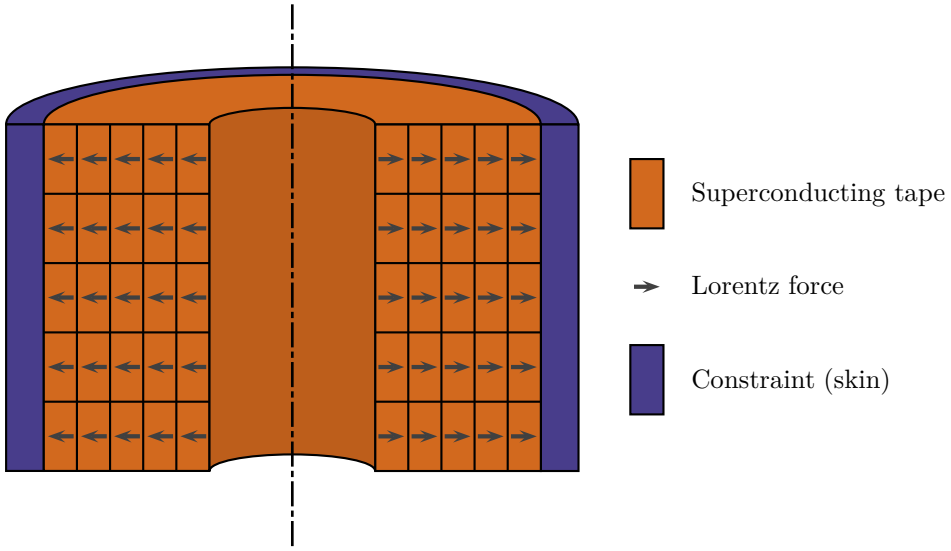

Figure 2.3: schematic of a constrained solenoid.

steel wrap. These hypotheses translate in two different boundary conditions:

Rigid constraint

In this case, the boundary conditions necessary to solve the Lamé equation are the following:

$$\sigma_{rr}(a) = 0$$

$$u_r(b) = 0$$

Elastic constraint

In this case the Lamé equation needs to be solved twice: the first time for the solenoid, the second for its radial support. The skin is not loaded by Lorentz forces, as it does not carry any current, but it is pushed by the solenoid. Then, defined p the pressure that occurs at the interface between solenoid and skin, the boundary conditions are:

$$\sigma_{rr}(a) = 0$$

$$\sigma_{rr}(b) = p$$

for the first equation, and:

$$\sigma_{rr}(a_s) = p$$

$$\sigma_{rr}(b_s) = 0$$

for the second one. Here a_s and b_s are respectively the inner and the outer radius of the skin. It can be noticed that $a_s = b$, as solenoid and skin are in contact, and $b_s - a_s = t_s$ which represent the skin thickness, or the amount of stainless steel wrapped around the coil. Also, this analysis does not include any skin pre-stress.

2.2.2 Material properties

At last, material properties have to be found and introduced into the analysis. This is not a trivial process, as there is a lack of literature about HTS mechanical properties, especially at the temperature of 4.2 K. These material are in fact interesting because they can work at 77 K, the temperature of liquid nitrogen, so most of the literature refers to that case.
For the coil, which is made of Superpower YBCO tape, the values relative to 77 K can be found in the company data sheets [54]:

- YBCO Young's modulus $E_t = 110\,\text{GPa}$.
- YBCO Poisson's ratio $\nu_t = 0.3$.

For the skin, it is crucial to choose a material with no possibilities of ferromagnetic behavior at 4.2 K. The best candidate is then the AISI 316 LN stainless steel, for which there is also plenty of literature and data at liquid helium temperature:

- AISI 316 LN Young's modulus $E_{SS} = 204\,\text{GPa}$.
- AISI 316 LN Poisson's ratio $\nu_{SS} = 0.3$.

Still, since the skin is made by a wound round filament, it is necessary to calculate an equivalent Young's modulus that takes into account the voids due to the packing of the wire. Figure 2.4 shows how to calculate this geometrical

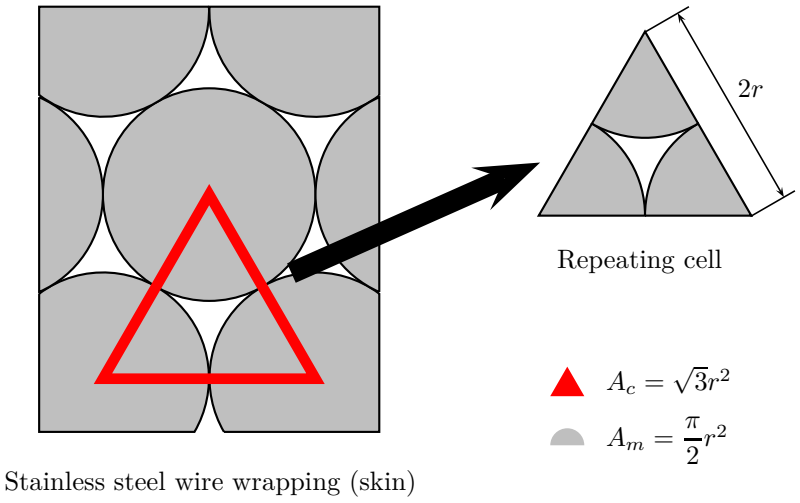

Figure 2.4: packing factor.

property in case of a round filament: the packing factor of the skin η_s is obtained by diving the area filled by the material A_m by the area of the repeating cell A_c. The value obtained is:

$$\eta_s = \frac{A_m}{A_c} = \frac{\pi}{2\sqrt{3}} \simeq 0.906 \tag{2.12}$$

which is used to define the skin Young's modulus $E_s = E_{SS} \cdot \eta_s$.
The Poisson's ratio is assumed to be the same of the original material $\nu_s = \nu_{SS}$. In conclusion the skin properties are:

- Skin equivalent Young's modulus $E_s = 185\,\text{GPa}$.
- Skin Poisson's ratio $\nu_s = 0.3$.

This simplification allows to calculate the strain correctly, but it underestimates the value of $\sigma_{\theta\theta}$ considering the whole area (steel strands and voids in between) as capable of carrying loads.
To obtain the correct stress value on the strands, the skin hoop stress obtained from equation 2.9 is divided by η_s.
In the radial and axial directions the calculation of the stress would become even more complicated, but considering how low these stresses are in comparison with the hoop stress; no intensification of stress is applied in these

directions. In conclusion, the skin material is considered homogeneous and isotropic: E_s and ν_s are adopted, and no stress intensification factor is applied; except to calculate $\sigma_{\theta\theta}$, which is divided by η_s.

2.2.3 Dimensions

The following insert solenoid dimensions are used in the analysis:

- $a = 9.5\,\text{mm}$.
- $b = 31\,\text{mm}$.
- $2l = 126\,\text{mm}$.
- $J = 5.21 \times 10^8\,\text{A/m}^2$.
- $a_s = b = 31\,\text{mm}$.
- $b_s = 35\,\text{mm}$.

These dimensions were defined during the previous study for a YBCO insert coil, and they are already optimized [55].

2.3 Results and conclusions

The equations above are coded into a computer program and solved numerically with the properties of the YBCO insert coil as input parameters. A similar study [56] also iterates this program, to optimize the dimensions of different solenoids.
Results in terms of stresses, calculated for $a \leq r \leq b_s$, are represented in figure 2.5. This plot shows that the point of the solenoid which is exposed to the maximum stress is located at the inner radius. Also, it can be noticed that the maximum value of tension is in the hoop direction ($\sigma_{\theta\theta}$), which means that the superconductor is mostly loaded along its own length.
It can also be noticed that the hoop stress is always greater than zero, while the radial stress (σ_{rr}) and the axial stress (σ_{zz}) are both positive and negative. This means that the superconducting tape is always in tension along its

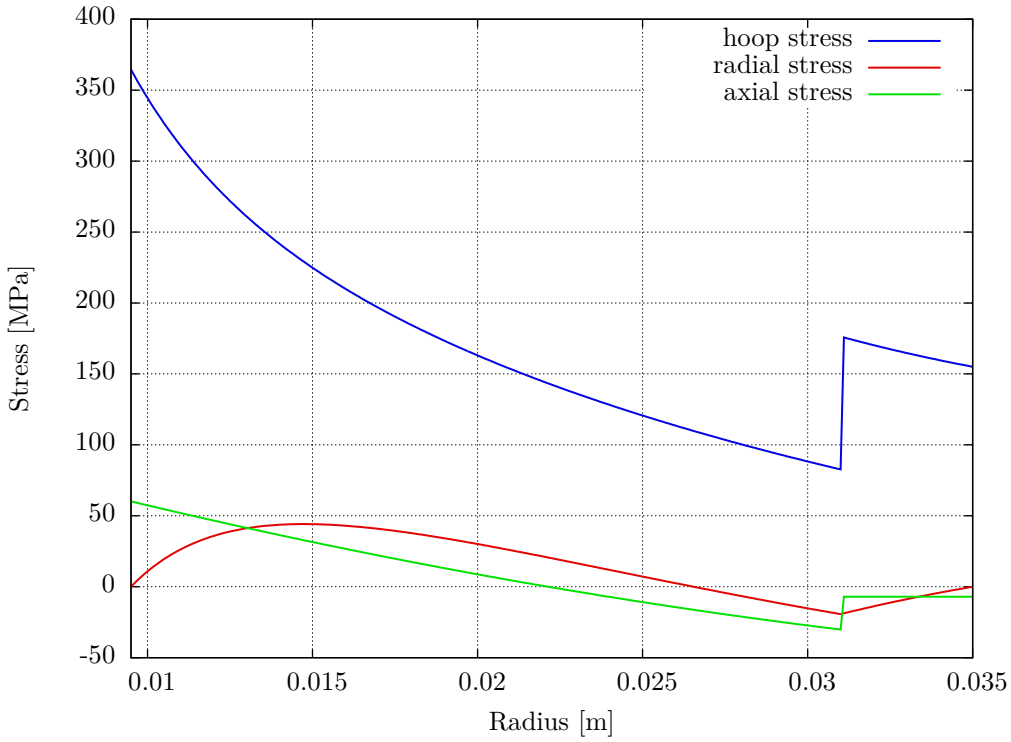

Figure 2.5: stress results on the solenoid mid-plane.

length, which is good in terms of mechanical stability, but there is a general tendency to detachment between some inner layers. This confirms that the choice to represent the coil as a solid material is correct, as long as the layers of superconductor are glued together. In fact, having a coil that is not glued would invalidate the hypotheses made before, leading to *instability* issues at the tape scale level.

An alternative to the resin impregnation could be given by a pre-stress compression state, achievable when tightening the skin around the coil, but this scenario is not investigated in this analysis. In fact this solution is heavily dependent on the thermal deformation that occurs when cooling the insert solenoid from room temperature to 4.2 K, and also on the tension induced in the tape and in the skin during their respective winding process, which cannot be precisely estimated yet.

However, the material properties adopted in the analysis refer to cryogenic

temperatures.
In conclusion, this analytical model shows that the maximum value of the stress ($\sigma_{\theta\theta} = 365\,\mathrm{MPa}$) is low compared to the value that the superconductor can withstand before showing degradation of its electrical properties, which is given [54] as about 700 MPa; and also the tension stress reached in the stainless steel skin, $\sigma_{\theta\theta} = 176\,\mathrm{MPa}$, is well below the yield limit of 922 MPa of the AISI 316 LN at 4.2 K [57].
These results demonstrate that from a structural point of view, the stainless steel wrap is an effective solution, definitely worth to be further investigated, and possibly adopted.
For all the above reasons, a more accurate finite elements analysis of the insert solenoid is performed, as described in the next chapter.

Chapter 3

The insert solenoid finite elements model

This part of the thesis work aims to evaluate more accurately the stress induced by Lorentz forces in the HTS solenoid and its stainless steel support, with the aid of several finite element models.
The first stage of this analysis is a magnetic simulation of both the insert and the outer magnet, to evaluate the total magnetic field generated and the resulting Lorentz forces; while the second stage focuses on the HTS insert only, determining the stresses and deformations induced by the Lorentz forces, in both the superconductor and its steel skin.
The commercial finite element software Ansys® Multiphysics™ v11.0 is used to perform these simulations.

3.1 The magnetic model

This first part of the simulation aims to obtain the total magnetic field generated by the two magnets, and consequently the Lorentz forces acting on the test coil, known its dimensions, the dimensions of the outer magnet and their operating currents.

3.1.1 Dimensions, materials and operating parameters

The insert geometry and its operating current density have already been summarized in Chapter 2. Here are reported the dimensions of the outer magnet as defined in the previous analyses [55]:

- External magnet inner radius 38.5 mm.
- External magnet outer radius 112 mm.
- External magnet total height 225 mm.
- External magnet current density $1.836 \times 10^8\,\mathrm{A/m^2}$.

Since all the chosen materials are non-magnetic even at the temperature of 4.2 K and since YBCO and the external magnet superconductors belong to the second type of superconductors, which allow magnetic field to pass through in quantized units of flux, the relative magnetic permeability μ_r of every material involved in the analysis is approximated as 1.

3.1.2 Finite element modeling and field results

Thanks to the axial-symmetry of the problem, a two-dimensional simulation is sufficient: the angular variable θ is omitted, and the whole model consists in a planar section in the two coordinates r and z.
In addition to that, there is also a plane of symmetry: the one that divides the solenoid and the outer magnet in two halves perpendicularly to their mutual axis. However, this symmetry is not exploited in the finite element model, because it is foreseen to use this simulation also to investigate the effects of a vertical *misalignment* of the magnets, occurring when the insert is not positioned correctly in the z direction, which leads to the loss of this symmetry.
The main element type used in this analysis is the `PLANE13` (2D coupled-field solid [58]) with the option of axial-symmetry.
There are two loads of current density, one on the test coil and one in the outer magnet, and the element correctly considers those current densities as

perpendicular to its own plane.
A second element type is adopted in the analysis: the `INFIN110` [58]. This element has the shape of a segment, and if attached to the border of a `PLANE13` elements mesh, it simulates an infinite air region beyond the mesh border itself. In fact, to model correctly the field generated by a solenoid, it should be necessary an infinite space to let the field expand and circulate freely at any distance from the coil. However, the necessity to limit the numbers of elements pushes the model to be as close as possible to the field sources. To prevent this from affecting the results, the `INFIN110` elements are placed at the border of the mesh to properly simulate an infinite region beyond the model limits. By a simulation point of view, the main effect is the reduction of the overall number of elements in the analysis, and therefore the reduction of the simulation computing time, without affecting the results quality.
Figure 3.1 shows the results of the magnetic analysis, in terms of magnetic field density modulus, expressed in T. The two rectangles are the insert solenoid and outer magnet sections. A change in the axes names has occurred: the mutual axis of the magnets z is called Y by the finite element software, and the radial axis r is referred as X.

3.1.3 Lorentz forces calculation

During the magnetic analysis solution, the software computes for each node the X and Y components of the Lorentz force (our r and z, respectively), and makes such results available in the `ETABLE` [58]. The force vector $\mathbf{F}_i$ acting on the i-esim node n_i is evaluated as:

$$\mathbf{F}_i = \left[\int_{S_i} J\left(X, Y\right) \mathrm{d}X \, \mathrm{d}Y\right] \hat{Z} \times \mathbf{B}_i \tag{3.1}$$

Where $\mathbf{B}_i$ is the magnetic field vector at the node, $J\left(X, Y\right)$ the current density of the adjacent elements and S_i is a part of the surface of the elements sharing the n_i node, according to figure 3.2. These results are then extracted and saved in a table containing the node number and the X and Y compo-

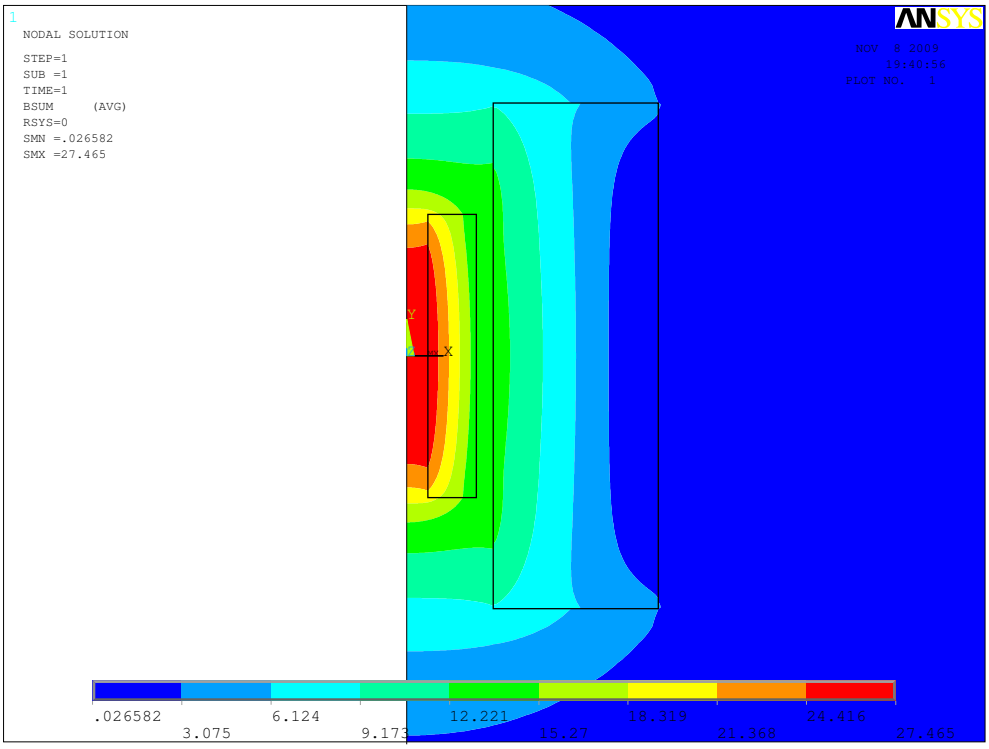

Figure 3.1: Ansys magnetic analysis results.

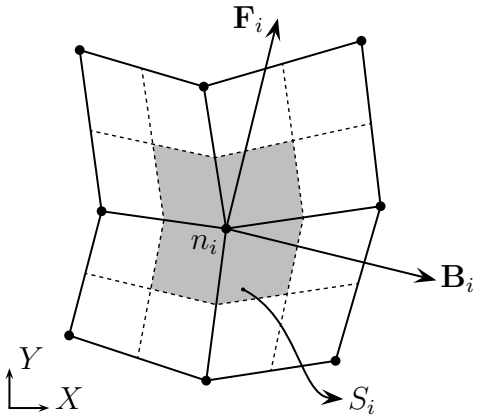

Figure 3.2: Lorentz force evaluation at the node n_i.

nents of $\mathbf{F}_i$ for each node of the insert solenoid. This is necessary because the whole magnetic mesh is discarded before the following mechanical analysis, and a new mesh based on different elements is created.
The magnetic analysis requires in fact a *continuous* mesh, to allow the magnetic field to circulate freely between adjacent regions of different materials; while the mechanical analysis needs *discontinuities* between the surfaces of the different bodies of the model, to perform a contact analysis. The element types used in the two simulations are also different.
However, if the mesh used for the mechanical analysis has exactly the same nodes names and locations as the magnetic analysis mesh, it is relatively simple to use a table of nodal Lorentz forces to transfer the correct loads from magnetic to mechanical analysis.
To guarantee that the node numbers and positions are the same in the two models, the insert solenoid mesh is the first to be created in both analyses, and the routine used to generate its nodes names and locations is the same.

3.2 The mechanical model

In principle, the superconducting coil is expected to expand and press again the surrounding stainless steel wrap, but since the whole structure is made of many different parts, and most of them are just pressed together, its complex behavior is difficult to predict *a priori*. For this reason, a complete *contact analysis* of the entire assembly is performed, with the assumption that every contact is unidirectional and cannot transmit any pressure unless in compression.

3.2.1 Contact analysis

The coil and the proposed support structure [55] are composed of several components made of different materials, as represented in figure 3.3. The majority of them are just packed together and held in place by the outer structure. For this contact analysis, every interface that lies between two parts made of different materials is modeled as a *gap*: each body is meshed with `PLANE42`

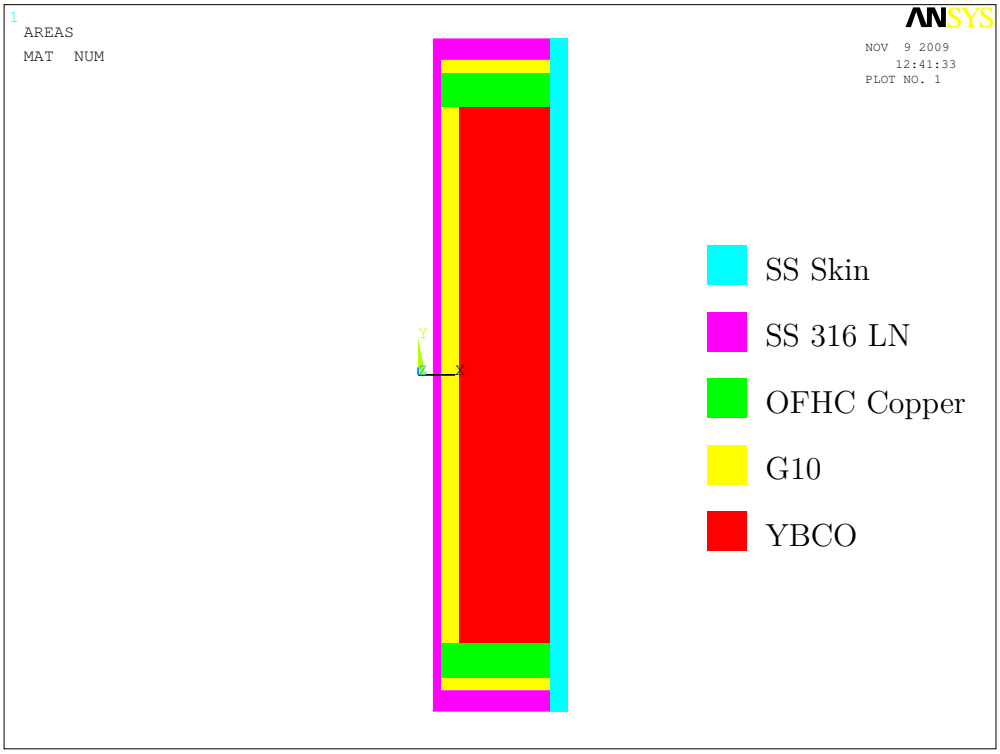

Figure 3.3: Ansys mechanical scheme.

elements [58], and the contact elements `CONTA171` and `TARGE169` [58] are placed at their interfaces.
The following material properties are adopted:

- OFHC Copper: E_c =138 GPa, $\nu_c = 0.34$.
- G-10: $E_g = 35$ GPa, $\nu_g = 0.2$.
- Stainless Steel (AISI 316 LN): $E_{SS} = 204$ GPa, $\nu_{SS} = 0.3$.
- Skin (wrap of Stainless Steel wire): $E_s = 185$ GPa, $\nu_s = 0.3$.
- Superconducting coil (YBCO): $E_t = 110$ GPa, $\nu_t = 0.3$.

The results of this contact analysis are represented in figure 3.4. The deformed shape of the assembly constituted by the coil and its support clearly shows the detached contact zones. The colors represent the equivalent mechanical stress, and the values on the scale are expressed in Pa. An agreement

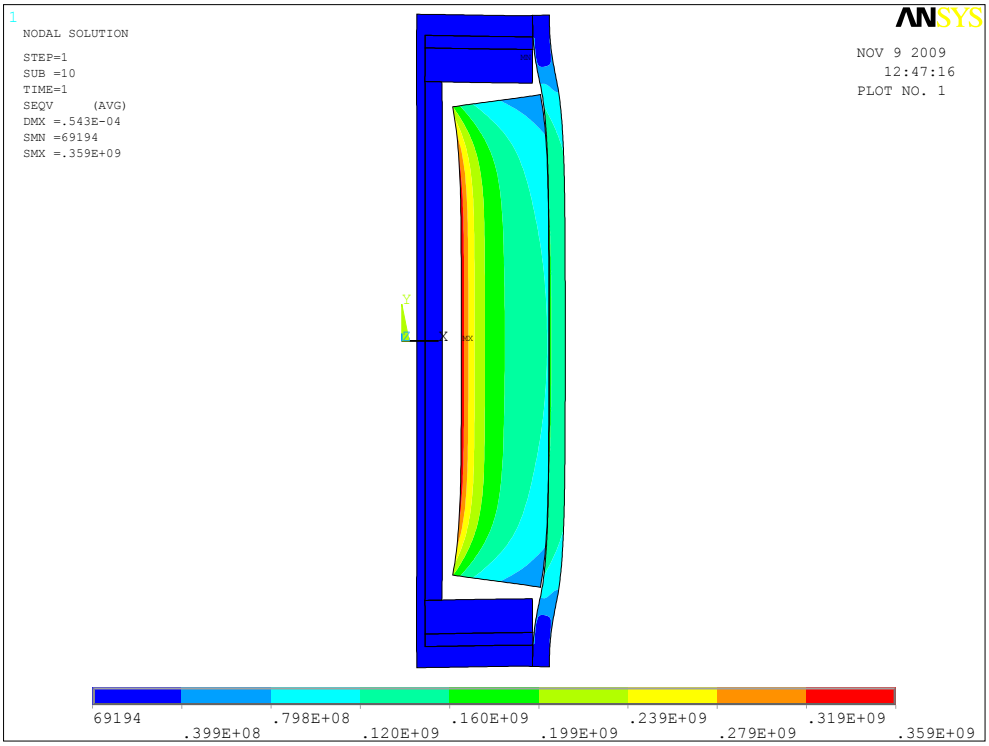

Figure 3.4: deformed shape and equivalent stress from contact analysis.

with the analytical model results is already evident, however the stress results are presented in greater detail at the end of this chapter.

3.2.2 Anisotropic model

The material constituting the coil is strongly anisotropic, therefore the mechanical analysis can be made more accurate by adopting an anisotropic material model for the solenoid. To define such material, the coil manufacturing process must be taken into account:

1. One side of the YBCO tape is *glued* to a thin layer of polyimide insulation, the commercial Kapton®.

2. The half-insulated tape is wound into a double pancake unit.

3. The double pancake unit is vacuum impregnated with CTD-101K epoxy resin and cured.

4. The desired number of double pancake units are piled and spliced together to form the complete insert coil.

As a consequence of this process, there is a sort of *elementary cell* which repeats itself within the whole coil: a section of YBCO tape, glued on one side to a piece of Kapton tape, with a small amount of epoxy resin filling the rest of the available space. A schematic of this cell is represented in figure 3.5.
This cell is studied to define the averaged mechanical properties of the compound material constituting the insert solenoid.

Elementary cell

Even if the magneto-mechanical model of the insert solenoid is two dimensional, due to the problem axial symmetry it is necessary to study a 3D elementary cell to obtain the three Young's moduli, the three Poisson's ratios and the shear modulus which are required (only one shear modulus is necessary, due to the axial symmetry).
The thickness, width and physical properties of the different materials that are included in this model are the following:

- Kapton: $0.0254\,\text{mm} \times 4.5\,\text{mm}$, $E_k = 5\,\text{GPa}$, $\nu_k = 0.34$.
- YBCO: $0.1\,\text{mm} \times 4\,\text{mm}$, $E_t = 110\,\text{GPa}$, $\nu_t = 0.3$.
- CDT-101K: $0.1\,\text{mm} \times 0.25\,\text{mm}$, $E_r = 2\,\text{GPa}$, $\nu_r = 0.35$.

The length of the cell is chosen as 0.1 mm, a value considered compatible with the thickness, however other values have been tested as well to ensure that this parameter is not affecting the results.
A mechanical 3D model is then created in Ansys, using `BRICK45` [58] elements, and four loading condition are defined, basing on the general form of

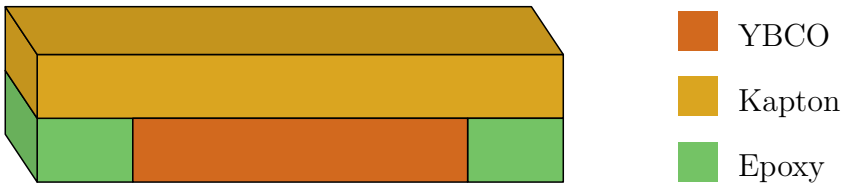

Figure 3.5: elementary cell schematic.

Hooke's law of elasticity for orthotropic materials:

$$\begin{Bmatrix} \varepsilon_{xx} \\ \varepsilon_{yy} \\ \varepsilon_{zz} \\ 2\,\varepsilon_{yz} \\ 2\,\varepsilon_{zx} \\ 2\,\varepsilon_{xy} \end{Bmatrix} = \begin{bmatrix} \frac{1}{E_x} & -\frac{\nu_{yx}}{E_y} & -\frac{\nu_{zx}}{E_z} & 0 & 0 & 0 \\ -\frac{\nu_{xy}}{E_x} & \frac{1}{E_y} & -\frac{\nu_{zy}}{E_z} & 0 & 0 & 0 \\ -\frac{\nu_{xz}}{E_x} & -\frac{\nu_{yz}}{E_y} & \frac{1}{E_z} & 0 & 0 & 0 \\ 0 & 0 & 0 & \frac{1}{G_{yz}} & 0 & 0 \\ 0 & 0 & 0 & 0 & \frac{1}{G_{zx}} & 0 \\ 0 & 0 & 0 & 0 & 0 & \frac{1}{G_{xy}} \end{bmatrix} \begin{Bmatrix} \sigma_{xx} \\ \sigma_{yy} \\ \sigma_{zz} \\ \sigma_{yz} \\ \sigma_{zx} \\ \sigma_{xy} \end{Bmatrix} \tag{3.2}$$

The loads conditions are defined as:

1. $\sigma_{xx} = 1\,\text{MPa}$.
2. $\sigma_{yy} = 1\,\text{MPa}$.
3. $\sigma_{zz} = 1\,\text{MPa}$.
4. $\varepsilon_{yz} = 1 \times 10^{-6}$.

Simulating these conditions and then substituting strains and stresses in equation 3.2 gives E_x, ν_{xy} and ν_{xz} in the first case, E_y, ν_{yx} and ν_{yz} in the second, E_z, ν_{zx} and ν_{zy} in the third, and finally G_{yz} in the fourth. G_{xy} and G_{zx} are not required due to the axial symmetry of the problem.
To model the first three loading conditions in the finite element model, three faces of the elementary cell are constrained in their normal direction (x, y and z), while the opposite three faces are left free to displace along their normal, with a condition: this displacement is imposed to be the same for each node belonging to the face, meaning that the planarity of the surface has to be conserved, and no rotations of the face are allowed. At this point,

a uniform pressure is applied on the movable face corresponding to the load case, then the model is solved to find the three values of ε_{xx}, ε_{yy} and ε_{zz}: the obtained values allow to determine the cell averaged Young's moduli and Poisson's ratios.
To determine the shear modulus in the fourth condition, it is instead preferable to impose the displacement as a load, and then calculate the resulting pressure on the external faces. This pure shear deformation load can be summarized with the following equation:

$$\begin{Bmatrix} U'_x \\ U'_y \\ U'_z \end{Bmatrix} = \begin{bmatrix} \cos\varepsilon_{yz} & \sin\varepsilon_{yz} & 0 \\ \sin\varepsilon_{yz} & \cos\varepsilon_{yz} & 0 \\ 0 & 0 & 1 \end{bmatrix} \begin{Bmatrix} U_x \\ U_y \\ U_z \end{Bmatrix} \tag{3.3}$$

Where $\mathbf{U}$ and $\mathbf{U}'$ are the position of each external node before and after the deformation, respectively.

Elementary cell results and validation

Simulating the materials properties and cell geometry specified above, and then substituting the results into equation 3.2, gives the following properties for the insert coil anisotropic material model:

- Young's moduli: $E_x = 25.8\,\text{GPa}$, $E_y = 25.4\,\text{GPa}$ and $E_z = 79.2\,\text{GPa}$.
- Major Poisson's ratios: $\nu_{xy} = 0.146$, $\nu_{zy} = 0.308$ and $\nu_{zx} = 0.312$.
- Shear modulus: $G_{xy} = 6.93\,\text{GPa}$.

To validate these results, a very simple analytical model is proposed. This model is based on combinations of springs, both in series and in parallel. Figure 3.6 shows two of these models, the ones relative to the deformation in the x and y directions. The elastic moduli obtained with these simple models are $E_x = 20.6\,\text{GPa}$, $E_y = 19.0\,\text{GPa}$ and $E_z = 79.2\,\text{GPa}$; showing an error with respect to the finite element meso-mechanical model of 5.4 GPa, 6.2 GPa and 0.0 GPa respectively.
These value suggest that the elementary cell model can be considered correct,

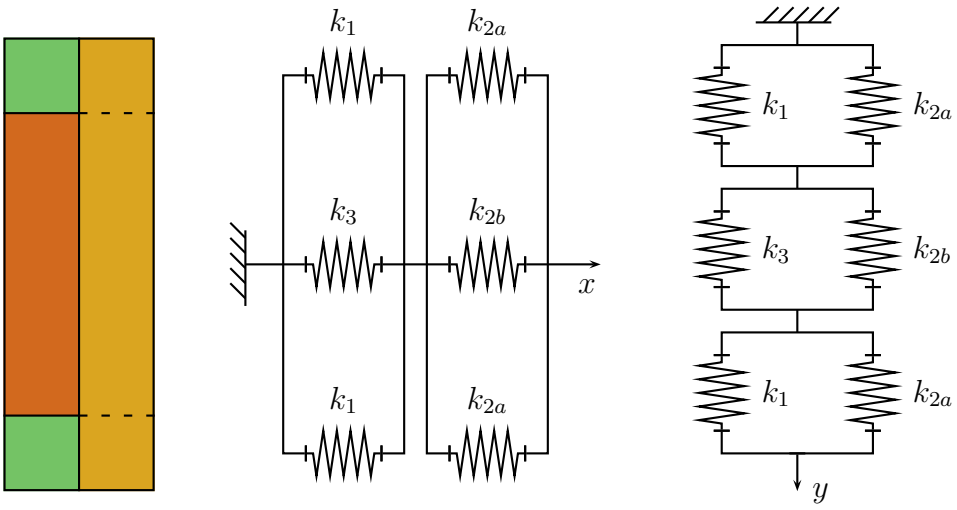

Figure 3.6: equivalent spring models to estimate the cell stiffness.

and all the calculated values of the Young's moduli, Poisson's ratios and the shear modulus are adopted as material properties for the insert solenoid in the complete magneto-mechanical simulation, taking into account that x, y and z in the reference system of the elementary cell correspond to r, z and θ in the reference system of the coil, respectively.

3.3 Finite elements models result summary

The complete magneto-mechanical simulation has been run twice, first with isotropic material properties, then with the calculated anisotropic ones. Furthermore, two additional runs have been performed with minor modifications, in order to estimate the effects of:

1. A vertical misalignment between the center of the insert solenoid and the center of the outer magnet.

2. The effects of different thermal contractions, that occur when the solenoid and its support are cooled in liquid helium.

All the results obtained are reported in the following paragraphs.

3.3.1 Isotropic model

Figure 3.7 shows the three principal stresses that occur in the midplane of the solenoid ($z = 0$), from the inner radius up to the outer (9.5 mm <= r <= 35 mm).
The value of hoop stress in the stainless steel skin is increased to take care of the skin packing factor, as already done in the analytical analysis.
A remarkable similarity with the analytical results is evident, with the hoop stress and the radial stress that differ at maximum by 12.5 MPa. The axial stress comparison shows a bigger difference, but this is expected, as the analytical model assumes a solenoid of infinite length, and therefore it cannot estimate correctly the vertical forces that arise at the extremities of the solenoid. At the top and bottom parts of the solenoid, in fact, the radial component of the field has the same magnitude of the axial component: since radial field generates axial forces on the coil, and these forces are neglected by the analytical model, the values of σ_{zz} resulting from the finite element models are more accurate, and should not be compared with the analytical ones.
According to this model the maximum hoop stress reaches 370 MPa in the coil, which is far from the maximum tension before electrical degradation of the tape, known to be as high as 700 MPa [59]. In the skin the maximum hoop stress reaches 176 MPa which is below the yield stress of AISI 316 LN steel, which is expected to be as high as 922 MPa at 4.2 K [57].

3.3.2 Orthotropic model

Using the properties obtained with the meso-mechanical model does not affect the general behavior of the solenoid, and in particular the contact area and the deformed shape remain substantially identical to the isotropic material case. The stress intensities however show a noticeable difference, as evident from figure 3.8.
Also in this case, the hoop stress in the skin is increased by dividing by the packing factor. Moreover, the stress in the coil is corrected by multiplying $\sigma_{\theta\theta}$ and E_t (tape Young's modulus) and then dividing by E_z (elementary

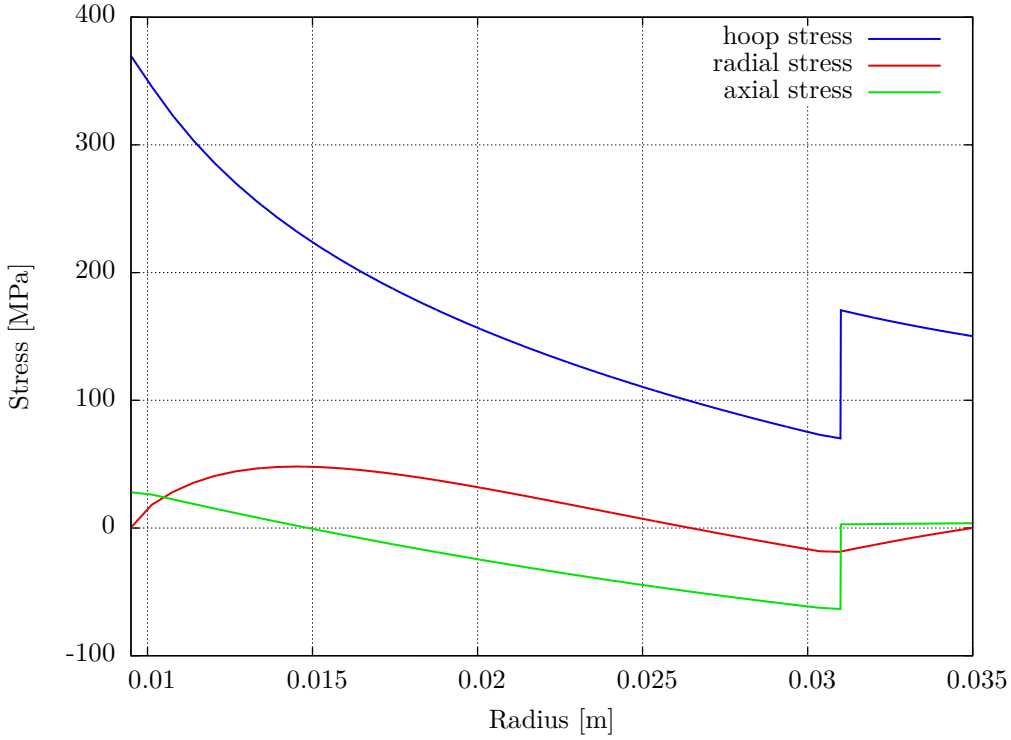

Figure 3.7: isotropic model stress results.

cell Young's modulus). This gives an estimate of the stress carried by the superconducting tape only, rather than the whole elementary cell. This adjustment is only applied to the hoop stress, and not to the radial and axial ones, due to the complexity of the mechanical stress distributions in these directions and due to their negligible absolute values.

The maximum hoop stress raises by about 248 MPa reaching 618 MPa in the superconductor and by about 33 MPa, reaching 209 MPa in the steel skin. Also the axial compression and radial tension increase, making the impregnation process of the solenoid more important, due to the increased possibility of a failure by delamination of the coil. As already mentioned in the analytical results paragraph, a pre-stress on the steel skin may help to reduce this phenomenon.

However, the conclusion of the finite elements mechanical analyses is that even when adopting the orthotropic material model, which is the most con-

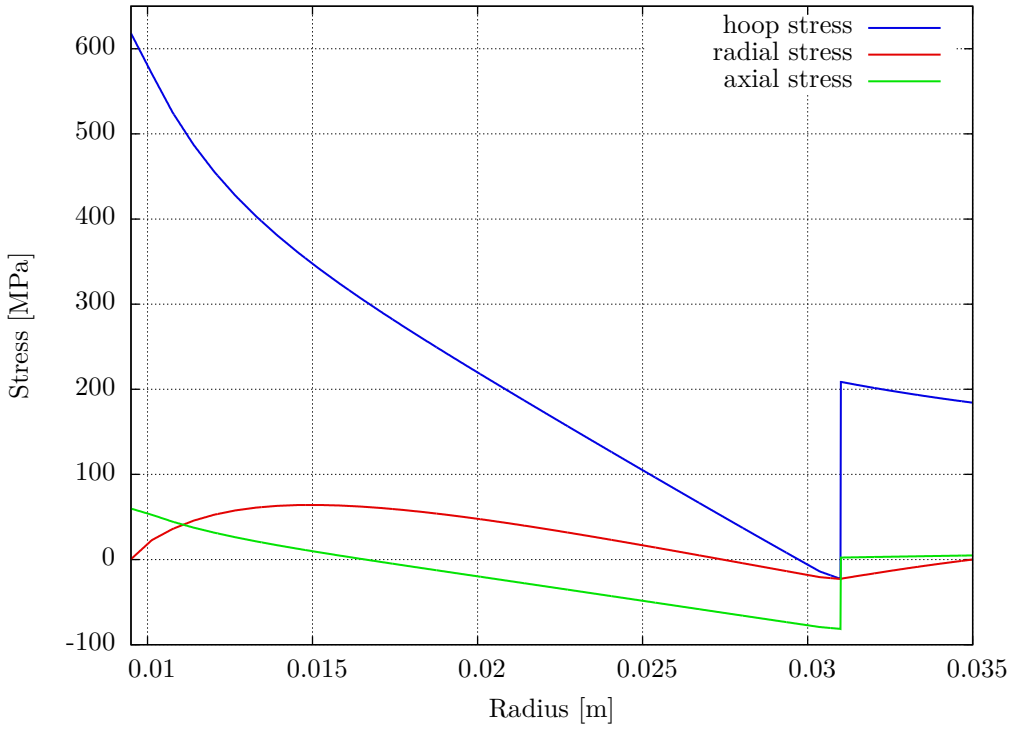

Figure 3.8: orthotropic model stress results.

servative being proposed so far; the maximum stresses allowable by superconductor and steel are not reached, making the insert coil and its support verified against Lorentz forces, even when operating at maximum current and maximum background field.

3.3.3 Thermal shrinkage and vertical misalignment

The temperature difference seen by the solenoid sensibly affects the stresses arising in the coil and skin, but the complexity of the problem and the lack of information about the tension that will be induced in the coil during the winding phase, prevent from having accurate results. However a rough estimate of the effects of thermal shrinkage is calculated assigning to the skin and the coil the integrated thermal contraction coefficients of steel and YBCO [60], respectively, and applying a thermal load of $-290\,°\mathrm{C}$ (the coil passes from about $20\,°\mathrm{C}$ to $4.2\,\mathrm{K}$). The result is a reduction of about $19\,\mathrm{MPa}$

in the coil hoop stress and an increase of 88 MPa in the skin. The superconductor seems to increase its safety margin, while the steel skin appears to be more loaded, but still remaining below the yield stress threshold.
However, more accurate thermal analyses are recommended as soon as the winding procedure and machinery become more defined.
Finally, the magneto-mechanical model is run with different displacements in the vertical direction between the centers of the two magnets. This is done to evaluate the effects of a possible vertical misalignment that could be generated by the wrong mating of the probe carrying the insert with respect to the outer magnet system. The results point out that the solenoids tend to *re-align* themselves, with a force of 1700 N/mm, for a linear displacement error within an interval of ± 15 mm.

Chapter 4

The HTS Insert Test Facility

The HTS Insert Test Facility (ITF) is the structure designed to support and operate the superconducting insert test coil, made of up to 14 double pancake units of YBCO tape. It provides mechanical support to the coil and its stainless steel skin; it also carries current leads, voltage taps and a Hall effect sensor. These are required to energize the test solenoid, measure the generated magnetic field and detect transitions of the superconducting state. The ITF is made mostly of stainless steel and copper, and has the shape of a probe, as shown in figure 4.1(a). It is designed to be operated within the Oxford Instruments® Teslatron® system, holding the test solenoid in its center. This system consists of a hybrid superconducting magnet which is contained in a larger cryostat, filled with liquid helium. Figure 4.1(b) shows the superconducting hybrid magnet in front of its own cryostat: the steel cylinder that lies on the floor, still partially frosted, contains a series of concentric solenoids made of NbTi and Nb_3Sn low temperature superconductors and can develop up to 14 T in a cold bore of 77 mm (16 T if operated at the helium λ point).

At the time this thesis started, an ITF prototype based on the previous study [55] was being manufactured by the Fermilab machine shop. The mechanical analyses performed during this work confirmed that the old design is still verified, even in light of the new hypotheses, however it was clear that some modifications were required in order to put it in commission.

(a) the HTS Insert Test Facility (ITF).

(b) superconducting magnet system of the Teslatron II, removed from its cryostat.

Figure 4.1: main hardware at the Superconducting R&D laboratory.

Although, for better understanding of the non-conformities analysis, and the consequent proposed modifications, it is worth to review the main objective of the ITF project.

4.1 Objectives of the ITF project at Fermilab

The purpose of ITF is to *develop technical knowledge* of HTS coil manufacturing and push forward the R&D of these materials, by overcoming the difficulties that arise during the design, assembly and operational phases of the facility itself.
In principle, ITF is expected to operate a HTS coil made of 14 YBCO double pancake units and develop a magnetic field of about 13 T in the background of 14 T, provided by the Oxford Instruments® Teslatron®.
Basing on the previous study [55] and considering the results of the mechanical analyses presented in chapter 3, the commissioning of the ITF is planned in three subsequent steps:

1. General test: insert the ITF inside the cryostat, check for leaks, shorts or other problems; if none, power a simple handmade double pancake unit made of just 3 turns of superconductor.

2. Whole double pancake: after verifying the ITF functionality, and after manufacturing the winding tooling to produce full double pancake units, use the facility to test a full double pancake.

3. Whole insert coil: after having verified more extensively the ITF, and after having designed a quench protection system for the insert solenoid, use the facility to test a full insert solenoid made of 14 double pancake units.

Considering the time already dedicated to the mechanical analyses, and the schedule for part delivery, this thesis work covers in full the first point, and also the design of the tooling equipment required for the second point.

4.2 The previous situation

Parts based on the first ITF design have been delivered in May 2009, but some issues need to be solved in order to put the ITF in commissioning. To better describe these issues, the ITF can be imagined as composed by three parts: top, center and bottom; each of them having its own functionality.

4.2.1 Upper part

The upper part of the ITF interfaces with the Teslatron II, the electrical power supply, the Hall effect sensor, two circular connectors for the voltage taps and an eye bolt for handling.
The interface with Teslatron II cryostat must guarantee adequate sealing and mechanical resistance at low temperature. The interface with the power supply consists in a couple of relatively heavy solid copper plates, which need to be supported by the stainless steel frame, while being electrically insulated from it. The ITF upper part carries two circular connectors to make available the voltage taps output to the acquisition system, and a Hall effect sensor to measure the field generated by the solenoid. The sensitive element however is mounted at the extremity of a rod which is as long as the ITF itself, as the measuring point is the center of the test coil, in the bottom part. Finally, an eye bolt is mounted on the upper part, to hook the ITS with an overhead crane, which is the safest way to handle it and insert it into the Teslatron II.

4.2.2 Central part

The central part consists in a long structure to provide physical support to the coil, and its length guarantees that the solenoid is placed at the right height inside the Teslatron magnet. Current leads and voltage taps wires are at the sides of the mechanical structure, which is composed by four stainless steel rods, welded to a series of horizontal plates constituting a sort of labyrinth for helium vapors, to reduce its consumption. The Hall effect sensor probe is in the center.

4.2.3 Lower part

Finally, the lower part is where the insert solenoid is held. The double pancake units are mounted on a pin, which is welded to the ITF main frame. The section of the pin is squared with rounded corners, to prevent any rotation of the pancakes.
After piling the desired number of double pancake units, as well as G-10 spacers to fill the remaining space, and two copper discs that are brazed to the current leads; the outer radii of pancakes and copper discs are joined together with splices made of wider YBCO tape. At last, the skin is wrapped around the whole solenoid, copper discs and spacers, and then secured to the ITF frame.

4.2.4 Non-conformities

It is evident that due to design or manufacturing errors, the upper part is not sealing adequately, and it is not strong enough to support the copper plates. Also, it cannot be equipped with an eye bolt.
On the central part, each of the four thin rods, constituting the principal structural support of the coil, is longer than the drawing specification. Also, the welding itself is only partially done, with evident lack of material.
Finally, on the lower part, the stainless steel skin results impossible to mount as it is manufactured as a solid piece.

4.3 Proposed solutions

In the upper part, non-conformities are solved by the design of four new pieces, of which the most complex is named Probe Top Sealing, shown in figure 4.2. It consists in a piece of solid G-10, a fiberglass-epoxy composite, with excellent behavior in terms of electrical insulation, mechanical resistance, machinability and resistance at low temperature. This component provides the support of the conducting plates, the sealing between cryostat and ambient and finally the support for the Hall effect sensor and circular connectors. It is compressed onto the ITF upper part, perpendicularly to

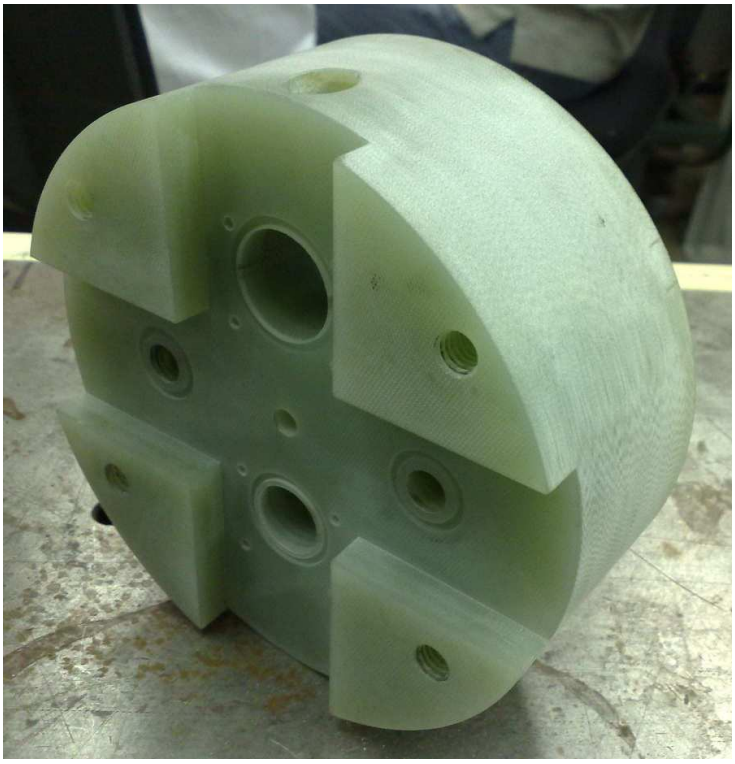

Figure 4.2: the new "probe top sealing" part.

its fiber planes, by a couple of bolts and a stainless steel arc, on which the eye-bolt is ensured. Thanks to the low pressure at which the cryostat operates, loads on this part are absolutely negligible. Figure 4.3 shows this new component mounted on the modified ITF upper part.
The problem on the probe length is not solved, as it does not affect the first two steps of the ITF project. In fact, even if the length is not correct, having only one double pancake instead of 14, allows to position the insert coil off-center with respect to the ITF, and therefore recover the error on the probe. For the same reason, for the first two steps of the ITF project, the non-conformity of the weldings does not constitute a problem either.
To replace the solid skin, instead of using a stainless steel wrap, which requires dedicated tools to be wound, it is proposed to use fiberglass tape, the commercial S-2 glass®, impregnated with CDT-101K epoxy resin and cured at 135 °C for 1.5 hours. Alternatively, the Stycast® 2850 FT epoxy can be

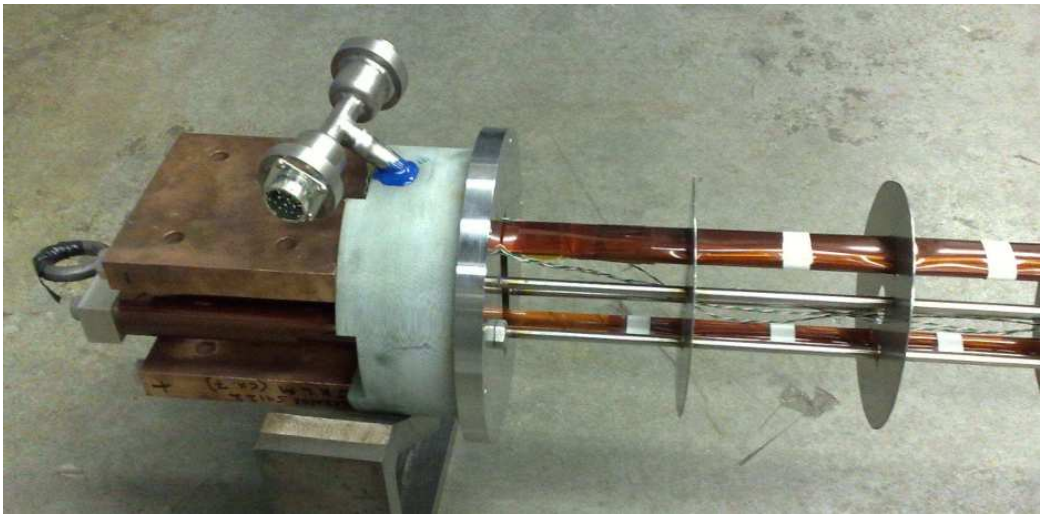

Figure 4.3: modified ITF upper part.

used together with the catalyst 23LV, which cures in about 24 hours at ambient temperature. This particular compound is easier to apply and cure, and therefore it is preferred to CDT-101K for the first tests. Figure 4.4 shows the ITF lower part with a coil installed covered by an S-2 glass and Stycast skin. This is a relatively reliable replacement, it can be wound by hand in the lab, and solves the problem of radial containment for the first step of the ITF project. For the next steps however, it is proposed to wrap the coil with stainless steel wire, in agreement with the mechanical analyses performed.

4.4 Commissioning and conclusions

In conclusion, all the new parts that are being proposed in this thesis work, are already approved, manufactured, installed and tested. Production drawings [61] are released in the Fermilab drawings archive.
ITF is operational, and the first phase of the project is ongoing, as experiments are being performed with small hand-wound test coils. The results are interesting, as fiberglass and epoxy containment allows to test every sample up to its superconducting-conducting transition. Also, subsequent experiments on the same test coils show consistently the same results, demon-

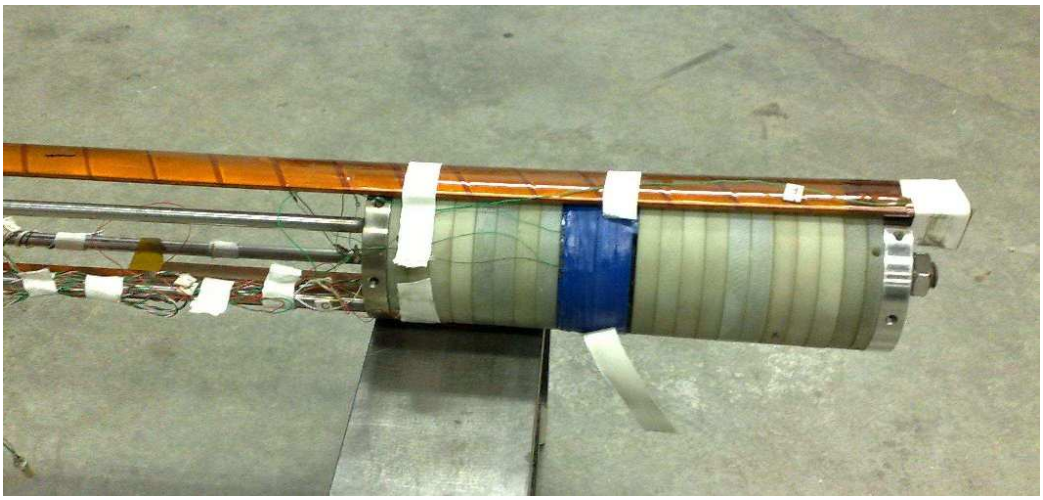

Figure 4.4: modified ITF lower part.

strating the absence of permanent mechanical damage, and therefore the reliability of the fiberglass-epoxy skin.

Chapter 5

The winding process and related tooling

As anticipated in the introduction and then seen in the ITF chapter, the insert solenoid is composed of a stack of double pancake units. Being the YBCO a superconductive *tape*, the easiest way to obtain a long solenoid out of it, is by stacking and connecting a series of single or double pancake units. The double pancake solution, compared to the single, does not need a splice at the inner radius to join together two consequent units, as the double pancake unit is composed of two single pancakes made out of the same continuous piece of tape, and therefore no joint is necessary at the inner radius. The disadvantage is that the winding process becomes more complex, as two different spirals having two opposite rotation senses need to be wound at the same time, from their common point at the inner radius.
However, as today, the splicing of HTS tapes is still considered a critical aspect of the coil manufacturing process, and because of that it is preferable to have a complex winding phase followed by an easier splicing phase rather than the opposite.

5.1 The double pancake

A double pancake is wound starting from its inner radius, and from the half of the total conductor length. For better understanding, it can be imagined that the midpoint of the overall tape length is placed on the pancake kernel, to form the helix that acts as link between the two spirals, as shown in figure 5.1(a). Once the helix is done, ideally, the two halves of the superconducting tape are wound in two different directions to form the upper and lower spirals of the double pancake unit, as shown in figure 5.1(b).
This procedure is good to understand the winding itself, but is not ideal from a manufacturing point of view. In particular, it is not practical to have two extremities of the superconductor in tension and rotating in opposite directions around a static kernel. It is more practical to have a rotating kernel and a fixed tensioner, and use these two devices to wind one spiral at the time. The complication of this method is that while winding the first spiral, the material required for the second one must be already spooled, cut, and held in a fixed position with respect to the rotating kernel.

5.1.1 The winding process

The procedure used to wind the double pancake is less straightforward than the one used to explain such kind of coils. The real coil in fact is wound by a single winding machine, which basically consists in a rotating spindle, and for its dimensions and functionality resembles a lathe; and a tensioner, which supplies new, insulated tape at the required tension.
What the two procedures have in common, however, is the starting point: in any case the double pancake *must* be wound starting from its inner radius and from the middle of the overall tape length. To achieve this task on a real winding machine, the first half of the superconducting tape is spooled onto a temporary bobbin fixed on the rotating spindle, as represented in figure 5.2(a). When enough tape is spooled, the temporary bobbin is removed from the center of the winding machine, and then fixed again on the same spindle, at a given distance from its rotation axis. At the same time the double pancake kernel is mounted at the center of the spindle, as shown in

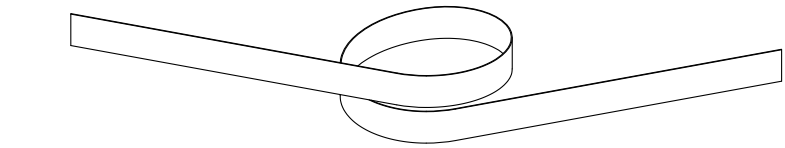

(a) helix is wound.

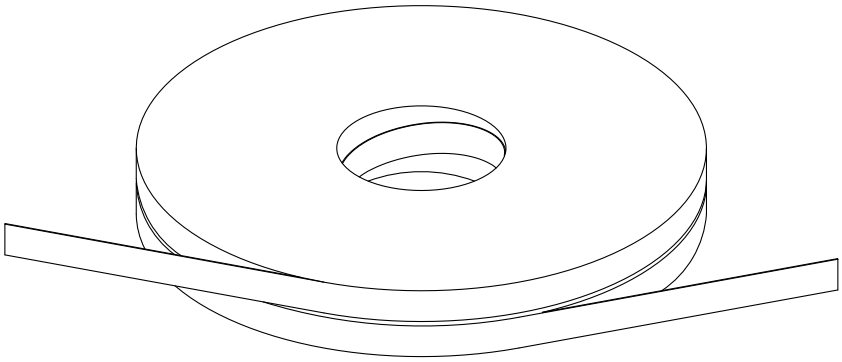

(b) spirals are wound.

Figure 5.1: conceptual winding of a double pancake unit.

figure 5.2(b).

From this configuration rotating the spindle allows to wind the tape around the double pancake kernel and obtain the helix located at the inner radius of the coil. The kernel also supports the double pancake and becomes an integrating part of it. Figure 5.3(a) shows this step in detail, illustrating how it is possible to wind the inner radius of the double pancake (the helix) while keeping the correct tension on the tape. During this step in fact one end of the superconducting tape is held in tension by the temporary bobbin, and the other by the tensioner.

After the helix is done, the entire spiral that lies further from the spindle is obtained by just spinning the winding machine. When completed, the tape coming from the tensioner is clamped on the spindle to ensure that the tension is kept, and then cut, as represented in figure 5.3(b).

Starting from this point in fact it is not necessary any more new material, as a spiral is wound and the material for the other one is coiled on the temporary bobbin. Therefore, the temporary bobbin is dismounted from the spindle and installed on the tensioner, in place of the original spool. Then the spindle is put in rotation again and the last spiral, the one closer to

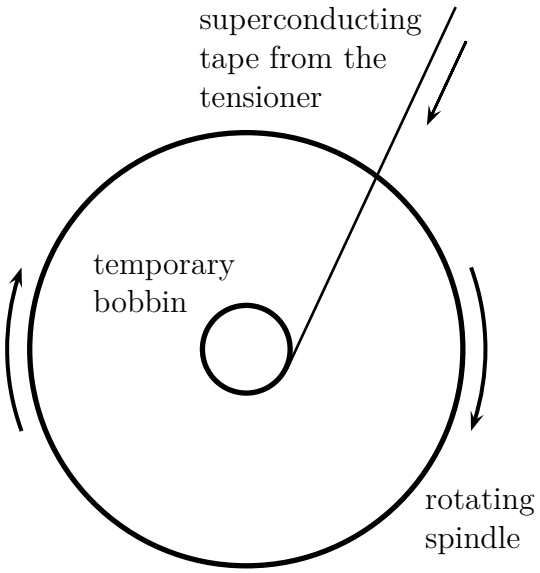

(a) first step: temporary bobbin is wound.

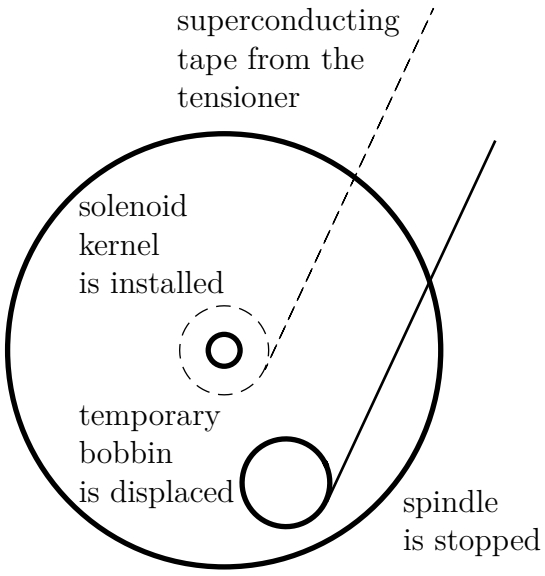

(b) second step: temporary bobbin is moved, solenoid kernel is installed.

Figure 5.2: winding schematic, part one: winding of the temporary bobbin and preparation of the double pancake winding.

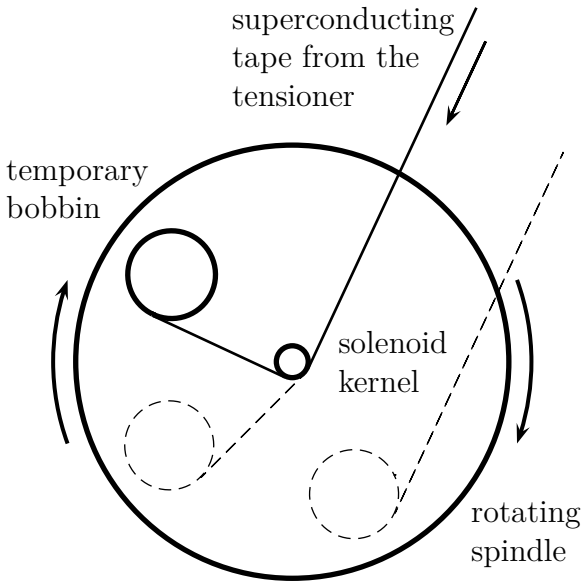

(a) third step: inner radius spiral is wound.

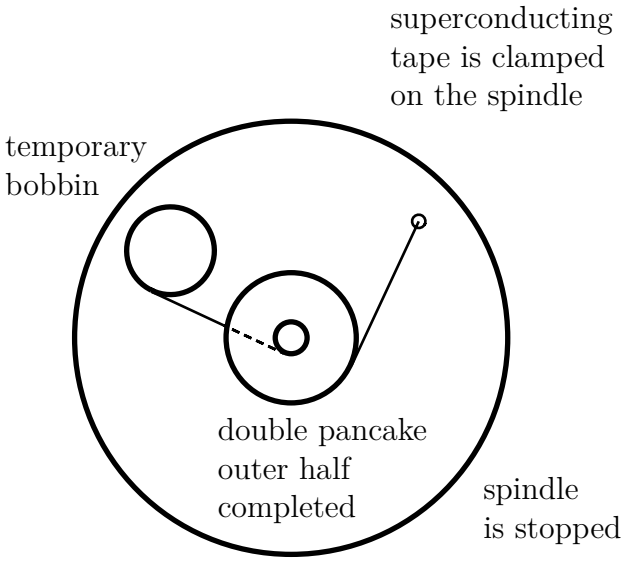

(b) fourth step: outer single pancake is wound and fixed.

Figure 5.3: winding schematic, part two: winding of the outer half of the double pancake and clamping of the wire extremity on the spindle.

the spindle, is wound. During this step however the sense of rotation of the winding machine is *inverted*, as figure 5.4(a) shows, as the two spirals have opposite senses.
Finally the end coming from the temporary bobbin, still fixed on the tensioner, is clamped onto the spindle to prevent any loss of tension in the double pancake, as represented in figure 5.4(b).
At this point the double pancake is completed and secured, then the whole fixture can be detached from the winding machine and sent to the polymer lab, where the coil can be impregnated with resin while its extremities are still clamped and in tension.

5.2 Winding tooling design

An entire set of tools is designed to carry on the series of operations described above. In practice, two devices are necessary:

1. The double pancake fixture, which is going to be attached to the winding machine spindle to support the auxiliary bobbin, the coil kernel and therefore the coil itself while being wound, as well as the clamps to hold in tension its tape extremities.

2. The pulleys for the tape routing and insulation, which support the tape while it travels from the tensioner to the winding machine, and at the same time apply the Kapton insulation layer to the superconductor.

5.2.1 Starting materials

The winding machine in use at the Fermilab coil workshop is a Broomfield model 350 [62], shown in figure 5.5. The only tensioner available consists in a vertical electric motor coupled to the superconductor spool by a magnetic clutch. A new, dedicated tensioner is also being evaluated for purchase.
The Kapton manufacturer provides the thin tape pre-glued and coiled on a cardboard kernel, having a nominal internal diameter of 3 inches. YBCO spools are made of aluminum and bronze, making them bigger and more

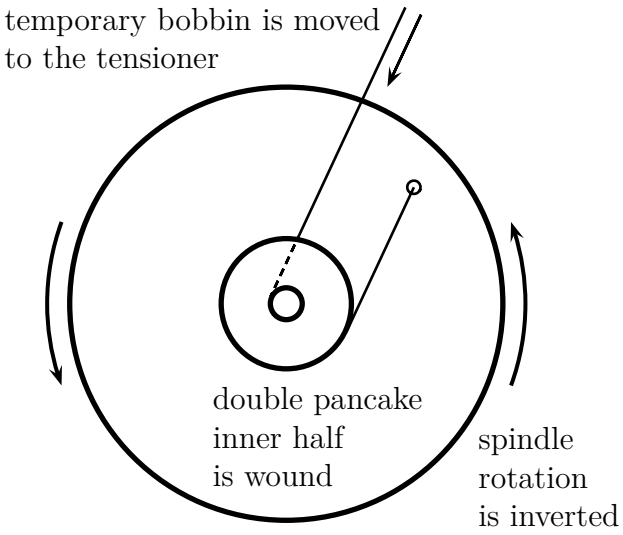

(a) fifth step: temporary bobbin is moved to the tensioner.

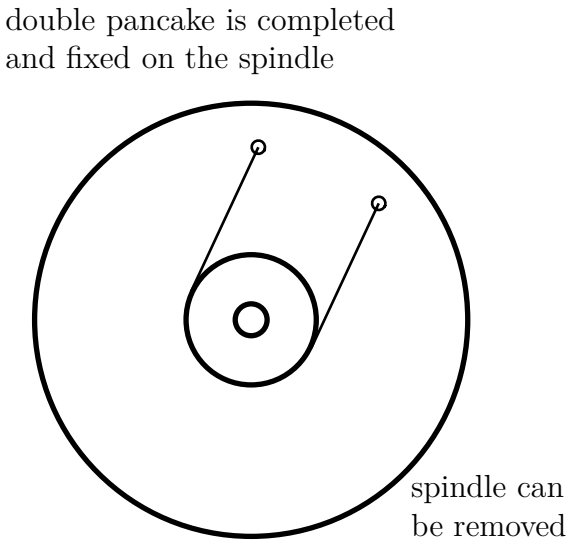

(b) sixth step: inner single pancake is wound and fixed.

Figure 5.4: winding schematic, part three: winding of the inner single pancake, clamping of the wire extremity and removal of the spindle.

Figure 5.5: the Broomfield winding machine.

robust, however their dimensions are not relevant as there is plenty of space on the currently available tensioner.

5.2.2 Insulation and routing pulleys

The winding machine is already equipped with its own set of pulleys, however a new set is designed to match the dimensions of the YBCO tape. These pulleys allow the insulation process to take place as well: the Kapton spool is fixed on a roller, then the insulation is routed into the same pulleys used by the superconductor, ensuring the contact between the two tapes as they travel through the same path, as represented in figure 5.6. The Kapton roller is idler, as the insulation is being pulled by the superconductor.
The dimensions of the pulleys grooves match the dimensions of YBCO and Kapton tapes, and the material chosen is a plastic, specifically Delrin® 100P BK602, to avoid any damage to the thin tapes and minimize the friction, even if the pulleys are mounted on ball bearings. Production drawings of this assembly have been approved and released into the Fermilab drawings archive [63], and the internal procurement procedure is launched.

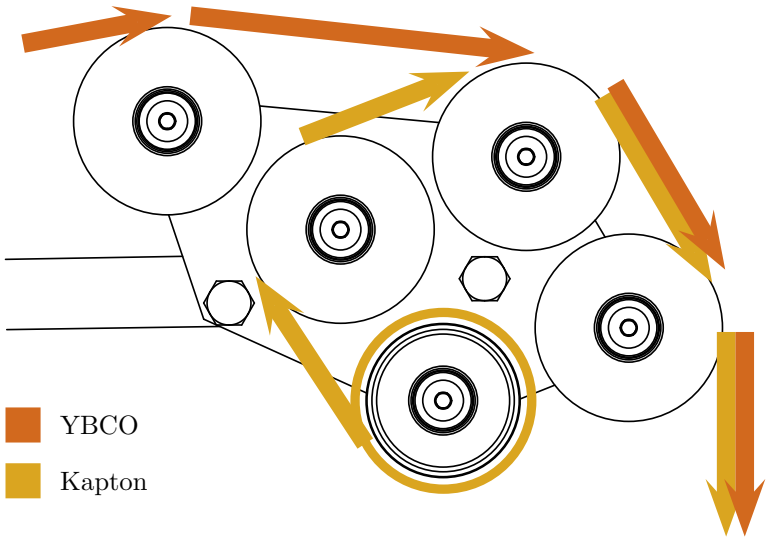

Figure 5.6: routing pulleys with insulation and superconductor routes.

5.2.3 The double pancake fixture

As anticipated previously, the double pancake fixture holds the double pancake while being wound, and therefore it must adapt to follow every different step of the winding process. To achieve this, the fixture is designed as an assembly of several different parts that can be mounted or dismounted in order to obtain the configurations required by each step. Figure 5.7 represents an exploded view of the complete double pancake fixture.

The main part is a base disc, which is referred to the winding machine spindle by means of dowel pins, and clamped to it.

On top of this disc, the temporary bobbin can be mounted in two positions: at the center, or with an offset of 2.375 inches.

The kernel holder can be mounted at the center of the base disc, to support the double pancake kernel. To prevent the kernel from rotating, the two mating profiles have the shape of a square with rounded corners, compatible also with the ITF pin.

An additional part is mounted and bolted onto the kernel holder to prevent the kernel from sliding along its axis: the upper clamp support. This part also supports the upper clamp, composed of two parts, which are going to provide support to the upper spiral tape end.

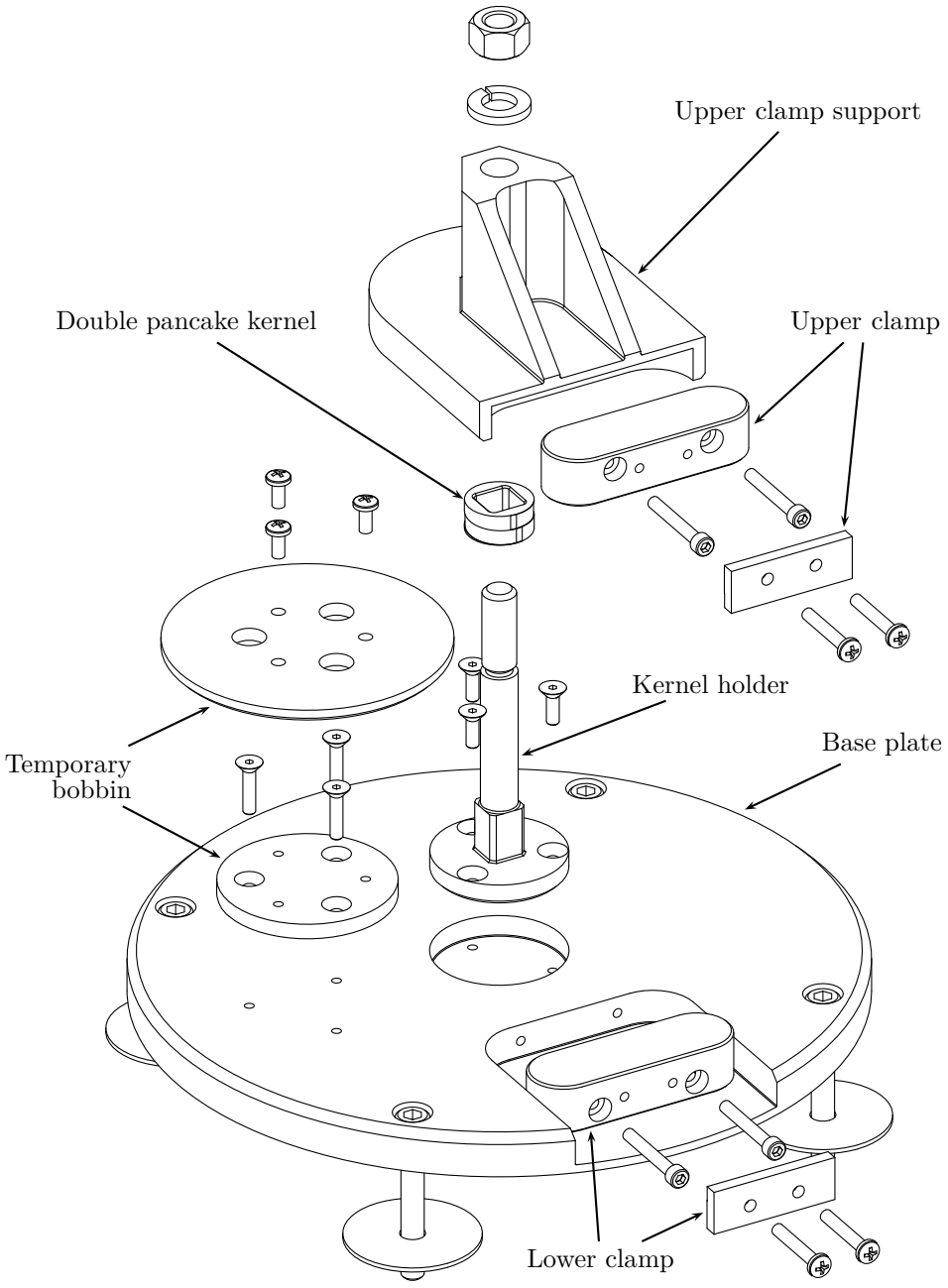

Figure 5.7: the double pancake fixture.

Finally the lower retaining clamp can be mounted on the base disc, to secure the lower spiral tape end.
All the parts represented are approved and released in the Fermilab drawings archives [63], and the procedure for internal procurement has already been launched, as well.

5.3 Conclusions

In conclusion, the drawings for the winding tooling are released and the parts are in production at the Fermilab machine shop. Delivery is expected for the end of January 2010.
For a better control over the tape tension, it could be necessary to purchase a dedicated tensioner with a tension range closer to the YBCO tape specifications, however the tensioner already present in the coil laboratory is compatible with the winding process, and the winding of the first pancake will start immediately after receiving the parts.

Chapter 6

Results and conclusions

To conclude this thesis work, all the results obtained are reported in this final chapter, together with some considerations and suggestions for the next steps of the superconducting R&D, carried on in the frame of the Fermilab High Field Magnets project.

6.1 Insert solenoid support and analyses

The stresses calculated with all the different models confirm that the mechanical resistance of the HTS coil and its support structure is a *critical* issue, as the self and mutual induced electromagnetic forces could limit the magnetic performances of the solenoid and even lead to mechanical failures, if underestimated. Therefore great attention must be given to the mechanical analyses, and to the support design.
The mesomechanical model remarks the importance of the structural behavior of the soft insulation materials interposed between turns of superconducting tape. Such material drastically changes the mechanical characteristics of the whole coil, and not necessarily in a favorable way: being the wound coil less stiff than expected, a greater amount of mechanical stress has to be supported by the outer skin. The external radial containment of the solenoid is then critical for its correct functioning.
Still, the 14 double pancake YBCO insert solenoid defined in the previous

steps of the project, and the new stainless steel skin wrapped around it to contain its deformation, are verified against mechanical failure as the safety coefficient remains below 1 even in the most conservative analyses. Nevertheless, the level of stress is higher than previously calculated, suggesting that the mechanical behavior of the solenoid is a complex problem, and it should be further investigated in the following steps of the high field magnet project, when bigger solenoids are going to be tested.
In particular it is suggested to investigate the internal stresses induced by cooling, as well as the ones introduced by the winding process; and then try to optimize the winding with the aim of having the most favorable internal stress state in the wound coil and skin.

6.2 ITF commissioning

The first step of the ITF project is successfully completed. The ITF is currently being operated to test HTS insert solenoids, insulated and wound by hand, and constituted of 3 turns of superconducting tape. For the radial containment, and S-2 glass and Stycast skin is being adopted.
When inserted and secured into the Teslatron II cryostat, no leaks, shorts or mechanical failures of any kind has been observed, and all the tests have been carried on successfully: each test coil has been powered up to its transition current for several times, proving that no irreversible mechanical damage occurred at the tape or splices level.
The current reached is still lower than the short sample limit previously measured for this kind of tapes, suggesting that there is margin of improvement in the manufacturing of the coil. A sensitive improvement is expected from the possibility to wind double pancake units with a winding machine, and not by hand. Another improvement could come from designing a tool to assist the splicing phase, and by defining a rigorous operational procedure for this delicate task. It is already decided that the next steps of the high field magnets project will focus on these improvements.

6.3 Double pancake winding

As for the winding, the design of the tooling has been approved, and the parts are being manufactured as this thesis goes to the press. Delivery is expected for the end of January 2010, and the winding of double pancake units could start immediately afterward, in the Fermilab coil workshop. At the same time, a dedicated tensioner is being evaluated for purchase, to improve the sensitivity of the tape tension settings. A decision will be taken after testing the winding with the current hardware.

6.4 Next steps

In conclusion, for the next steps, it is proposed to extend the detail of the mechanical analyses, by including the effects of the winding tension for both the coil and the stainless steel skin, which could be controlled to achieve a defined pre-stress state in the solenoid and its support, aiming to minimize the stresses during operation.
For the ITF it is proposed to strengthen the current probe or even manufacture a new one, to carry on the third phase of the ITF project. In fact, the non-conformities on the current structure do not allow to test more than one double pancake unit at the time. However, the current version of the ITF has a great potential in terms of experiments, as it could be used to investigate different kinds of supporting skins, and to solve the issue of the splicing techniques. For this last topic, a possible solution could be the design of a splicing tool, or the developing of detailed procedures, to obtain a more consistent splice quality.
As a final note, it is necessary to develop a dedicated quench protection system in order to test a full YBCO insert test coil, as the energy stored in a full insert solenoid is enormous, and it should be damped quickly and efficiently in case of quench, to avoid any damage to the outer magnet and cryostat, other than to the test coil itself.
High Field Magnet project at Fermilab is an ambitious project and therefore it is constantly facing impressive challenges, however high temperature

superconductors are promising materials that show an incredible potential. Their technical limits and their possible applications are still to be fully understood, making this kind of research extremely stimulating and interesting.

Bibliography

[1] J. G. Bednorz and K. A. Müller, "Possible high T_c superconductivity in the Ba-La-Cu-O system," *Condensed Matter*, vol. 64, pp. 189–193, 1986.

[2] J. Bardeen, L. N. Cooper, and J. R. Schrieffer, "Theory of superconductivity," *Physical Review*, vol. 108, pp. 1175–1204, 1957.

[3] R. Eisberg, *Quantum physics of atoms, molecules, solids, nuclei, and particles*. New York: Wiley, 1985.

[4] M. Buchanan, "Mind the pseudogap," *Nature*, vol. 409, pp. 8–11, 2001.

[5] A. J. Leggett, "What DO we know about high T_c?," *Nature Physics*, vol. 2, pp. 134–136, 2006.

[6] C. Caroli, P. G. D. Gennes, and J. Matricon, "Bound fermion states on a vortex line in a type II superconductor," *Physics Letters*, vol. 9, no. 4, pp. 307–309, 1964.

[7] Y. Kamihara, H. Hiramatsu, H. Hosono, M. Hirano, T. Kamiya, R. Kawamura, and H. Yanagi, "Iron-based layered superconductor: LaOFeP," *J. Am. Chem. Soc.*, vol. 128, no. 31, pp. 10012–10013, 2006.

[8] Y. Kamihara, T. Watanabe, M. Hirano, and H. Hosono, "Iron-based layered superconductor La[$O_{1-x}F_x$FeAs ($x = 0.05 - 0.12$) with $T_c = 26$ K]," *J. Am. Chem. Soc.*, vol. 130, no. 11, pp. 3296–3297, 2008.

[9] H. Takahashi, K. Igawa, K. Arii, Y. Kamihara, M. Hirano, and H. Hosono, "Superconductivity at 43 K in an iron-based layered compound $LaO_{1-x}F_xFeAs$," *Nature*, vol. 453, no. 7193, pp. 376–378, 2008.

[10] R. Zhi-An, "Superconductivity and phase diagram in iron-based arsenic-oxides $ReFeAsO_{1-\delta}$ (Re = rare-earth metal) without fluorine doping," *Europhysics Letters*, vol. 83, p. 17002, 2008.

[11] G. Wu, Y. L. Xie, H. Chen, M. Zhong, R. H. Liu, B. C. Shi, Q. J. Li, X. F. Wang, T. Wu, Y. J. Yan, J. J. Ying, and X. H. Chen, "Superconductivity at 56 K in samarium-doped SrFeAsF," in *Hefei National Laboratory for Physical Science at Microscale and Department of Physics*, (Hefei, Anhui 230026, China), March 2009.

[12] M. Rotter, M. Tegel, and D. Johrendt, "Superconductivity at 38 K in the iron arsenide $(Ba_{1-x}K_x)Fe_2As_2$," *Physical Review Letters*, vol. 101, no. 10, p. 107006, 2008.

[13] K. Sasmal, B. Lv, B. Lorenz, A. M. Guloy, Feng Chen, Y.-Y. Xue, and C.-W. Chu, "Superconducting Fe-based compounds $(A_{1-x}Sr_x)Fe_2As_2$ with A=K and Cs with transition temperatures up to 37 K," *Physical Review Letters*, vol. 101, no. 10, p. 107007, 2008.

[14] M. J. Pitcher, D. R. Parker, P. Adamson, S. J. C. Herkelrath, A. T. Boothroyd, R. M. Ibberson, M. Brunelli, and S. J. Clarke, "Structure and superconductivity of LiFeAs," *Chem. Commun*, pp. 5918–5920, 2008.

[15] J. H. Tapp, Z. Tang, B. Lv, K. Sasmal, B. Lorenz, P. C. W. Chu, and A. M. Guloy, "LiFeAs: An intrinsic FeAs-based superconductor with T_c=18 K," *Physical Review B*, no. 78, p. 060505, 2008.

[16] D. R. Parker, M. J. Pitcher, P. J. Baker, I. Franke, T. Lancaster, S. J. Blundell, and S. J. Clarke, "Structure, antiferromagnetism and superconductivity of the layered iron arsenide nafeas," *Chem. Commun.*, pp. 2189–2191, 2009.

[17] F.-C. Hsu, J.-Y. Luo, K.-W. Yeh, T.-K. Chen, T.-W. Huang, P. M. Wu, Y.-C. Lee, Y.-L. Huang, Y.-Y. Chu, D.-C. Yan, and M.-K. Wu, "Superconductivity in the PbO-type structure α-FeSe," *Proceedings of the National Academy of Sciences USA*, vol. 105, no. 38, pp. 14262–14264, 2008.

[18] J. Zhao, Q. Huang, C. de la Cruz, S. Li, J. W. Lynn, Y. Chen, M. A. Green, G. F. Chen, G. Li, Z. Li, J. L. Luo, N. L. Wang, and P. Dai, "Structural and magnetic phase diagram of $CeFeAsO_{1-x}F_x$ and its relation to high-temperature superconductivity," *Nature Materials*, vol. 7, no. 12, pp. 953–959, 2008.

[19] C. H. Lee, A. Iyo, H. Eisaki, H. Kito, M. T. Fernandez-Diaz, T. Ito, K. Kihou, H. Matsuhata, M. Braden, and K. Yamada, "Effect of structural parameters on superconductivity in fluorine-free $LnFeAsO_{1-y}$ (Ln = La, Nd)," *J. Phys. Soc. Jpn.*, no. 77, p. 083704, 2008.

[20] A. Hebard, M. Rosseinsky, R. Haddon, D. Murphy, S. Glarum, T. Palstra, A. Ramirez, and A. Kortan, "Superconductivity at 18 K in potassium-doped C_{60}," *Nature*, 1991.

[21] A. Ganin, Y. Takabayashi, Y. Khimyak, S. Margadonna, A. Tamai, M. Rosseinsky, and K. Prassides, "Bulk superconductivity at 38 K in a molecular system," *Nature Materials*, vol. 7, no. 5, pp. 367–371, 2008.

[22] N. W. Ashcroft, "Metallic hydrogen: A high-temperature superconductor?," *Phys. Rev. Lett.*, vol. 21, pp. 1748–1749, Dec 1968.

[23] J. Lindenhovius, E. Hornsveld, A. den Ouden, W. Wessel, and H. ten Kate, "Powder-in-tube (PIT) Nb_3Sn conductors for high-field magnets," *IEEE Transactions on Applied Superconductivity*, vol. 10, no. 1, pp. 975–978, 2000.

[24] B. A. Glowacki, M. Majoros, M. E. Vickers, and B. Zeimetz, "Superconducting properties of the powder-in-tube Cu-Mg-B and Ag-Mg-B wires," *Physica C: Superconductivity*, vol. 372-376, no. Part 2, pp. 1254 – 1257, 2002.

[25] T. Beales, J. Jutson, L. LE, *et al.*, "Comparison of the powder-in-tube processing properties of two $(Bi_{2-x}Pb_x)$ $Sr_2Ca_2Cu_3O_{10+\delta}$ powders," *Journal of material chemistry*, vol. 7, no. 4, pp. 653–659, 1997.

[26] Y. Ma, Z. Gao, Y. Qi, X. Zhang, L. Wang, Z. Zhang, and D. Wang, "Fabrication and characterization of iron pnictide wires and bulk materials through the powder-in-tube method," *Physica C: Superconductivity*, vol. 469, no. 9-12, pp. 651 – 656, 2009. Superconductivity in Iron-Pnictides.

[27] K. Marken, H. Miao, M. Meinesz, B. Czabaj, S. Hong, S. Technol, O. Instruments, and N. Carteret, "BSCCO-2212 conductor development at Oxford Superconducting Technology," *IEEE Transactions on Applied Superconductivity*, vol. 13, no. 2 Part 3, pp. 3335–3338, 2003.

[28] H. Liu, S. Dou, K. Song, and C. Sorrell, "Superconducting properties of Au/Bi-Pb-Sr-Ca-Cu-O composites," *Superconductor Science and Technology*, vol. 3, pp. 210–212, 1990.

[29] H. Miao, K. Marken, M. Meinesz, B. Czabaj, S. Hong, S. Technol, O. Instrum, and N. Carteret, "Development of round multifilament Bi-2212/Ag wires for high field magnet applications," *IEEE Transactions on Applied Superconductivity*, vol. 15, no. 2 Part 3, pp. 2554–2557, 2005.

[30] C. Briant, E. Hall, K. Lay, and J. Tkaczyk, "Microstructural evolution of the BSCCO-2223 during powder-in-tube processing," *Journal of Materials Research*, vol. 9, no. 11, pp. 2789–2808, 1994.

[31] H. Miao, K. Marken, M. Meinesz, B. Czabaj, and S. Hong, "Round Multifilament Bi-2212/Ag wire development for high field magnet applications," in *Materials Science Forum*, vol. 546-549, pp. 1927–1930, Transtec Publications; 1999, 2007.

[32] K. Goretta, M. Lanagan, J. Singh, J. Dusek, U. Balachandran, S. Dorris, and R. Poeppel, "Fabrication of high-T_c superconductors," *Materials and Manufacturing Processes*, vol. 4, no. 2, pp. 163–175, 1989.

[33] A. Goyal, D. P. Norton, D. K. Christen, E. D. Specht, M. Paranthaman, D. M. Kroeger, J. D. Budai, Q. He, F. A. List, R. Feenstra, H. R. Kerchner, D. F. Lee, E. Hatfield, P. M. Martin, J. Mathis, and C. Park, "Epitaxial superconductors on rolling-assisted biaxially-textured substrates (RABiTS): a route towards high critical current density wire," *Applied Superconductivity*, vol. 4, no. 10-11, pp. 403 – 427, 1996.

[34] Y. Iijima, N. Tanabe, Y. Ikeno, and O. Kohno, "Biaxially aligned $YBa_2Cu_3O_{7-x}$ thin film tapes," *Physica C: Superconductivity*, vol. 185, pp. 1959–1960, 1991.

[35] M. Rupich, X. Li, C. Thieme, S. Sathyamurthy, S. Fleshler, D. Tucker, E. Thompson, J. Schreiber, J. Lynch, D. Buczek, *et al.*, "Advances in second generation high temperature superconducting wire manufacturing and R&D at American Superconductor Corporation," *Superconductor Science and Technology*, vol. 23, p. 014015, 2010.

[36] Y. Xie, D. Hazelton, J. Llambes, Y. Chen, X. Xiong, A. Rar, K. Lenseth, Y. Qiao, A. Knoll, J. Dackow, and S. V, "Recent developments in 2G HTS wire and its application in superconducting power equipment," in *22nd International Symposium on Superconductivity (ISS2009)*, (Tsukuba, Japan), November 2009.

[37] V. Lombardo, E. Barzi, G. Norcia, M. Lamm, D. Turrioni, T. Van Raes, and A. Zlobin, "Study of Hts Insert Coils for High Field Solenoids," in *AIP Conference Proceedings*, vol. 1218, p. 246, 2010.

[38] D. Neuffer, "Colliding muon beams at 90 GeV," *Particle Accelerators*, vol. 14, p. 75, 1983.

[39] J. Gallardo, R. Palmer, A. Tollestrup, A. Sessler, A. Skrinsky, *et al.*, "Muon Muon Collider: Feasibility Study," *eConf*, vol. C960625, p. R4, 1996.

[40] C. Ankenbrandt, "Status of muon collider research and development and future plans," *Phys. Rev. ST Accel. Beams*, vol. 2, p. 081001, 1999.

[41] A. Jansson, "Muon accelerator R&D program: A proposal for the next 5 years." unpublished, November 2008.

[42] S. Geer, "Neutrino beams from muon storage rings: Characteristics and physics potential," *Phys. Rev.*, vol. 57, no. 11, pp. 6989–6997, 1998.

[43] N. Holtkamp and D. Finley, "A feasibility study of a neutrino source based on a muon storage ring," *Fermilab Publications*, vol. 00, no. 108, 2000.

[44] S. Geer and H. Schellman, "Physics at a neutrino factory," *Fermilab Notes*, no. 692, p. 8064, 2000.

[45] A. D. Rujula, M. B. Gavela, and P. Hernandez, "Neutrino oscillation physics with a neutrino factory," *Nucl. Phys.*, vol. 547, no. 21, 1999.

[46] S. Osaki, R. Palmer, M. Zisman, and J. Gallardo, "Feasibility study ii of a muon-based neutrino source," *BNL-52623*, 2001.

[47] S. Geer and M. Zisman, "The neutrino factory and beta beam experiments and development," *APS Neutrino Study*, 2004.

[48] S. Geer and M. Zisman, "Neutrino factories: Realization and physics potential," *Prog. in Part. and Nucl. Physics*, vol. 59, p. 631, 2007.

[49] A. Bross, "The Neutrino Factory," in *FERMILAB-CONF-09-169-APC (PAC09)*, vol. FR3RBI04, 2009.

[50] A. Bandyopadhyay, S. Choubey, R. Gandhi, S. Goswami, B. Roberts, J. Bouchez, I. Antoniadis, J. Ellis, G. Giudice, T. Schwetz, *et al.*, "Physics at a future Neutrino Factory and super-beam facility," *Reports on Progress in Physics*, vol. 72, p. 106201, 2009.

[51] Muon Collider Study Group, "Muon collider advanced accelerator R&D proposal." unpublished, 2009.

[52] M. N. Wilson, *Superconducting magnets*. Oxford scientific publications, 1983.

[53] S. Timoshenko, *Strength of Materials*, vol. II. D. Van Nostrand Company, 1956.

[54] D. W. Hazelton, "2G HTS high field magnet demonstration," tech. rep., Superpower Inc., 2007.

[55] G. Norcia, "Design of modular test facility for high temperature superconductor insert coils," Master's thesis, Università degli Studi di Pisa, 2008.

[56] E. Terzini, E. Barzi, and V. Lombardo, "Analytical study of stress state in HTS solenoids," tech. rep., Fermilab Technical Division, 2009.

[57] D. Larbalestier, "Selection of Stainless Steel for the Fermilab Energy Doubler Saver Magnets," 1977.

[58] ANSYS, Inc., *ANSYS® Multyphisics, Release 11.0, Help System*, 2009.

[59] D. Hazelton, "Recent developments in YBCO for high field magnet applications," in *Presentation at the Low Temperature Superconductivity Workshop (LTSW 2008)*, (Tallahassee, FL, USA), November 2008.

[60] D. Hazelton, V. Selvamanickam, J. Duval, D. Larbalestier, W. Markiewicz, H. Weijers, and R. Holtz, "Recent developments in 2g hts coil technology," *Applied Superconductivity, IEEE Transactions on*, vol. 19, pp. 2218–2222, June 2009.

[61] A. Bartalesi, "`ER# 9539`." Fermilab drawings archive, 2009.

[62] Broomfield, *Model 350 specifications*, 2007.

[63] A. Bartalesi, "`ER# 9605`." Fermilab drawings archive, 2009.